OPTICAL REMOTE SENSING TECHNIQUES TO ESTIMATE PHYTOPLANKTON CHLOROPHYLL a CONCENTRATIONS IN COASTAL

Chapter · January 2006

DOI: 10.1007/1-4020-3968-9_3

1 author:

John Schalles
Creighton University
51 PUBLICATIONS **2,370** CITATIONS

SEE PROFILE

Chapter 3

OPTICAL REMOTE SENSING TECHNIQUES TO ESTIMATE PHYTOPLANKTON CHLOROPHYLL *a* CONCENTRATIONS IN COASTAL WATERS WITH VARYING SUSPENDED MATTER AND CDOM CONCENTRATIONS

JOHN F. SCHALLES
Biology Department, Creighton University, Omaha, NE 68178, USA,
jfsaqua@creighton.edu

1. Introduction

"Roughly 98% of the world's oceans and coastal waters fall into the Case 1 category, and almost all bio-optical research has been directed toward these phytoplankton-dominated waters. However, near-shore and estuarine Case 2 waters are disproportionately important to human interests such as recreation, fisheries, and military operations. It is therefore likely that Case 2 waters will receive increasing attention in coming years." – Curtis Mobley, 1994. Light and Water: Radiative Transfer in Natural Waters

The estimation of chlorophyll concentrations is one of the most scientifically relevant and commonly used applications of remote sensing to aquatic coastal systems. This, however, is a far from trivial task because of the complex composition and distribution of optically active constituents in many coastal waters. In the decade since the publication of Mobley's "Light and Water", the hydrologic optics of turbid Case 2 waters (Morel and Prieur, 1977) have been vigorously examined. The advantages and challenges of remote estimation of chlorophyll concentrations in Case 2 waters are now relatively well defined, although operational monitoring schemes are not fully mature and await further sensor and algorithm improvements (International Ocean-Color Coordinating Group, 2000). This chapter will survey this important component of coastal remote sensing. There is much to be gained from examining the commonalities in the optical environments of inland and coastal water, and I will draw primarily from empirical studies that span these diverse and optically complex environments. This chapter also considers the transferability of the well developed, satellite remote sensing approaches for chlorophyll assessments of open ocean, Case 1 waters (O'Reilly et al., 1998) to Case 2 waters.

The terminology and rationale for Case 1 and Case 2 water classifications were established by Morel and Prieur (1977) in their seminal work on the bio-optical basis for ocean color variations. The optics and emergent color signals of Case 1 waters are largely dominated by: 1) living phytoplankton cells; 2) organic tripton (detritus) particles from death and decay of phytoplankton and the grazing products of zooplankton; and 3) the dissolved organic matter produced by phytoplankton metabolism, and decay of organic tripton (modified from Gordon and Morel, 1983). Case 2 waters contain Case 1 constituents plus materials introduced from outside the water column, which also effect optical properties. These include: 4) turbulent resuspension of bottom particles in shallow areas; 5) inorganic and organic tripton from river drainages, glaciers, and/or wind transport; 6) terrigenous and littoral zone colored dissolved organic matter (CDOM); and 7) anthropogenic particulate and dissolved

L.L. Richardson and E.F. LeDrew (eds.), Remote Sensing of Aquatic Coastal Ecosystem Processes: Science and Management Applications, 27-79.

substances (Klemas and Polis, 1977; Gordon and Morel, 1983; Alberts and Filip, 1994; Bukata et al., 1995). Although Case 1 conditions normally prevail offshore, they may also occur: 1) in coastal and near shore areas in arid regions, where shelf geology is limited and deep water occurs just off the coastline; 2) during droughts resulting in highly reduced or no runoff; or 3) other instances where currents introduce offshore water in localized areas lacking significant terrestrial runoff. Obviously, Case 2 conditions intergrade spatially with Case 1 conditions in relation to distance from coastlines and river plumes. Physical dynamics and seasonality can result in state changes for a given location. The chlorophyll prediction algorithms for Case 1 and Case 2 waters are often different, and both sets may be required in coastal zones. Note that certain *in situ* water column processes (ex. phytoplankton blooms or amplified scattering by carbonates from coccolithophores or whiting events) can shift the optics of offshore waters away from true Case 1 conditions.

Most approaches for remote estimation of phytoplankton biomass are based on the absorption of sunlight by algal pigments in the presence of light scattering by algal cells and non-algal particles. This interplay of pigment-specific absorption and particle scattering produces graded responses in the emergent reflectance signals detectable by radiometer instruments. This chapter will examine the nature of these graded responses and their utilization in various quantitative and qualitative assessment schemes for spatial and temporal patterns of phytoplankton abundance.

Coastal, estuarine, and inland water habitats present serious challenges to the interpretation of diagnostic light signals because of the diversity of optically active constituents, which partially mask fundamental phytoplankton absorption and scattering relationships (Carder et al., 1989; Gallegos et al., 1990; Ritchie et al., 1994; Schalles et al., 1998a). Field spectroscopy measurements in turbid inland and coastal Case II waters have increased substantially in the past decade (Wang et al, 1996; Kahru and Mitchell, 1998; Dekker et al., 1997; Schalles et al., 1998a, 1998b; Gitelson et al., 2000; Cunningham et al., 2001; Lahet et al., 2001; Gons et al., 2002; Brando and Dekker, 2003; Dall 'Olmo et al.,2003). These and similar studies have led to the production of new chlorophyll prediction algorithms for Case 2 waters. Several Case 2 algorithms are operational for sensors on aircraft (Kallio et al., 2003) and satellites (Ruddick, 2004).

The chlorophyll algorithms for Case I waters (Gordon and Morel, 1983; O'Reilly et al., 1998) are universally based on a simple interaction of phytoplankton density with water - as cell densities increase, chlorophyll and carotenoid absorptions increasingly dominate at blue wavelengths and generally cause decreased reflectance, whereas cell scattering increasingly dominates at mid-green wavelengths and causes increased reflectance (see detailed explanations below). A simple blue to green ratio has a robust and sensitive relationship to chlorophyll *a* concentrations in Case I waters. The relationship becomes less sensitive at higher chlorophyll levels (above ~ 30 µg/l chl *a*). The relationship is also sensitive to changes in the ratios of chlorophyll *a* (hereafter, chl *a*) to total algal pigment and total carotenoids (Aiken et al., 1995). Furthermore, this simple relationship can be highly compromised by the effects of CDOM and/or tripton particles in turbid, Case II estuarine and near shore waters and even waters well offshore in regions of large river plumes. For example, the influence of the Orinico plume can extend across the entire central Caribbean (Muller-Karger et al., 1989). CDOM material in the Orinoco plume caused significant overestimation of chlorophyll using Coastal Zone Color Scanner (CZCS) data. In many estuaries, CDOM and tripton dominate the optical processes of water column components (Bowers et al., 2003). Cole and Cloern (1987) estimated that phytoplankton accounted for only 5% of light attenuation in South San Francisco Bay. Biogenous calcite can substantially increase

water reflectance, particularly from resuspension of carbonate sediments during stormy periods and the mass appearance of coccoliths during the declining stages of coccolithoporid blooms (Brown and Yoder, 1994) and extensive "whiting" conditions in inland lakes and coastal and offshore waters.

2. Chlorophyll as an Integrative Bioindicator

Chl *a* is the dominant light harvesting pigment and is universally present in eukaryotic algae and the Cyanophyceae (cyanobacteria or "bluegreen algae") (Rowan, 1989). The only potential water column phototrophs lacking chl *a* are certain photosynthetic bacteria such as Purple or Green bacteria, which contain bacteriochlorophylls with different absorption maxima, and phototrophic Archaebacteria containing bacteriorhodopsin as the light-harvesting pigment.

Chl *a* is commonly measured in water quality monitoring programs for coastal and inland waters (Jordan et al., 1991; Morrow et al., 2000;, Cracknell et al., 2001;, Casazza et al., 2003), in surveillance programs for harmful algal blooms (Munday and Zubkoff; Paerl, 1988; Richardson, 1996; Kahru and Mitchell, 1998;, Pettersson et al., 2000), and in ecological studies of phytoplankton biomass and productivity (Cole and Cloern, 1987; Talling, 1993;, Gallegos and Jordan, 2002; Lefevre et al., 2003). The contribution of phytoplankton derived primary production on continental margins (shelves, slopes, and rises) to both global ocean production and particulate organic carbon export to the deep oceans has been underexamined, but appears to be highly significant (Walsh, 1991; Jahnke, 1996).

It is important to keep in perspective that remote measurements of *in situ* phytoplankton using passive solar reflectance are generally incapable of isolating the chlorophyll signal from other cell components and other optically active compounds (OACs) in the water column. Even the chlorophyll fluorescence signals detected by active LIDAR systems can be affected by other fluorescing materials, red reabsorption by chl *a* and optical processes of the extracellular environment (Doerffer, 1993; Pozdnyakov et al., 2002). Chl *a* is packaged with other pigments within the refractive and reflective contents of algal cell walls, membranes, and other cytoplasm constituents. An extensive analysis (n ~ 5600 stations) of ocean pigment data found an average total pigment to chl *a* ratio of 2.164, with a range of 1.876 to 2.876 across cruises and ocean provinces (Aiken et al., 1995).

Uniform sphere models of cells are unable to reasonably describe scattering in marine phytoplankton cells (Quinby-Hunt et al., 1989). A three layered model using a high refraction index for the outer layer (cell wall component) and low indices for middle (chloroplasts) and inner (cytoplasm) layers performed well in simulating a mixed particle size distribution from the central Pacific gyre (Kitchen and Zaneveld, 1992). Non-extractive, remote sensing schemes to detect and monitor phytoplankton chlorophyll must contend with the complex scattering and absorbing features of this total cell package. In most natural assemblages, cell populations of mixed species with variable shapes and sizes (submicron to tens of microns or more) and differing cell wall constituents and pigment suites occur in spatially heterogeneous patterns. Other photosynthetic and photoprotective pigments have overlapping spectral absorption with chl *a*, especially at the blue, Soret band of chlorophyll (Figure 1). An example of an aggregate absorption spectrum (chl *a* plus accessory chlorophylls and carotenoids) is compared to an isolated chl *a* spectrum in Figure 2. The data in Figure 2 were produced using the specific absorption coefficients of Bidigare et al. (1990; see Figure 1) and a

global ocean average of the proportions of each of the five classes of pigments from Aiken et al. (1995). Note that the data in Figure 2 are scaled to a chl *a* concentration of 1 µg/l. Between about 460 and 570 nm, accessory pigments account for most absorption. Even at 440 nm, accessory pigments account for 52% of the total absorption. However, above 600 nm chl *a* absorption is dominant, and accounts for nearly all absorption above 650 nm. Most notable is the *in vivo* red absorption maximum of chl *a* at 674 nm (Figure 2). Chl *a* pigment absorption is present but barely detectable in the range of about 698 to 730 nm. In this spectral range, specific absorption coefficients decrease from 0.0010 to 0.0001 m^2 * mg^{-1} (Bidigare et al., 1990).

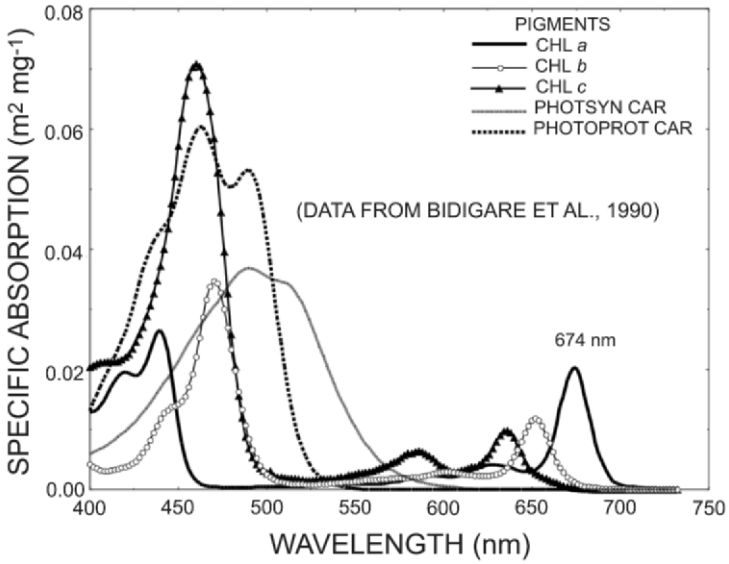

Figure 1. Calculated *in situ*, weight specific absorption coefficients for the major phytoplankton pigments: chl *a, b, c* = chlorophylls *a*, *b,* and *c*, Psyn Car = photosynthetically active carotenoids, Pprot Car = photoprotective carotenoids. Note red absorption maximum for chl *a* at 674 nm.

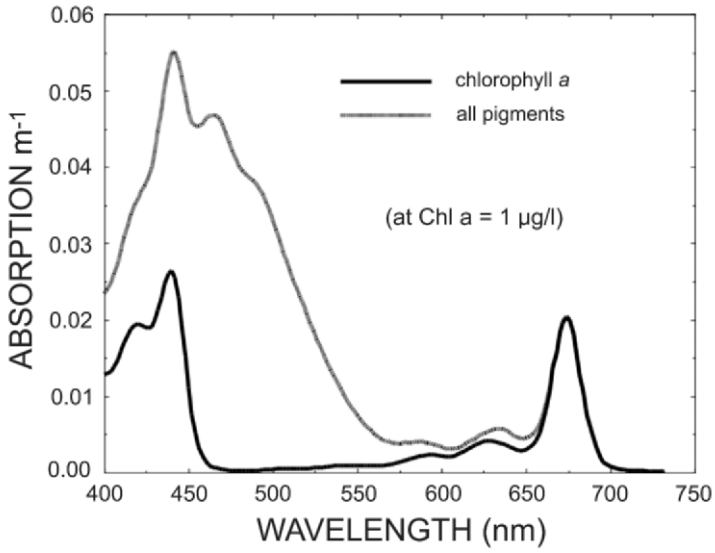

Figure 2. Comparison of *in situ* chl *a* absorption (at a chl *a* concentration of 1 µg/l) versus total pigment absorption (with all chlorophylls and carotenoids) based on the specific absorption coefficients for five pigment classes (Figure 1) and global ocean averages for the proportions of these five classes (see text).

Chlorophyll distribution may have significant vertical variation, particularly when stable stratification develops in coastal and estuarine waters (Paerl, 1988) or with the characteristic deep chlorophyll maximum of oligotrophic ocean waters (Lefevre et al., 2003). Optical remote sensing above the water surface generally cannot resolve deep chlorophyll layers and other vertical heterogeneity patterns (Andre, 1992). A further complication, rarely considered, arises when multiple wavelength algorithms use bands representing differing optical depths. For example, in a turbid eutrophic water column, blue and red reflectance signals attenuate much more rapidly (in both the down and upwelling fields), and the composite upwelling blue and red signals return from shallower depths than the green signals.

Chlorophyll is a comparatively efficient and effective, albeit indirect, measure of phytoplankton biomass. There are three primary analytical approaches for laboratory analyses of chl *a* concentration in field samples: spectrophotometry, fluorometry, and high-performance liquid chromatography (American Public Health Association, 1998). Most analyses begin with filtration of the chlorophyll-containing pigment fraction. Pigments are then extracted with an organic solvent (acetone, methanol, or less commonly ethanol or diethyl ether (Rowan, 1989). Freezing, grinding, and other techniques to physically disrupt algal cells generally improve the extraction pigment yield. Note that these extraction schemes also bring accessory pigments (except for the water soluble phycobiliproteins) into solution. Following clarification of the extract with filtration or centrifugation, the pigment content is assessed using pigment specific absorption bands in a spectrophotometer, via fluorescence using proper excitation and emission wavelength settings, or through chromatographic column separation (usually HPLC) together with in-line optical detection of column fractions. HPLC is now widely used to simultaneously identify and quantify the entire suite of extractable

pigment fractions. These techniques provide both direct estimation of pigment in samples and calibration information for *in situ* measures.

In situ chl *a* is currently assessed using fluorometry (submersible or shipboard probes or airborne LIDAR systems; see Yoder et al., 1992), wavelength specific path attenuation in transmissometers (Morrow et al., 2000), and measurement of water column reflectance from close range, airborne (Kallio et al., 2003), or satellite sensors (Brando and Dekker, 2003). When data are collected from high altitude aircraft and satellite sensors, the signal from water column reflectance is usually far lower in magnitude than the atmospheric scatter. Removal of this "atmospheric effect" through correction techniques is very important for standardizing data and normalization to reflectance (Bukata et al., 1995; Gordon, 1997; Brando and Dekker, 2003).

Antoine et al. (1996) used CZCS satellite data to estimate an average chl *a* value of 0.19 µg/l for the world's oceans. These workers further calculated that 55.8% of the world's oceans (between 50°S to 50°N) averaged less than 0.1 µg/l chl *a*, 41.8% were between 0.1 and 1 µg/l, and only 2.4% exceeded 1 µg/l, levels which they classified as oligotrophic, mesotrophic, and eutrophic, respectively. In the low phytoplankton densities of the open oceans, productivity is comparably low. On average, the quantum yield in the oceans is about one third that of terrestrial ecosystems, with only one CO_2 molecule fixed per 1500 incident photons (Falkowski and Raven, 1997).

Most coastal waters exceed the 0.19 µg/l chl *a* average, with more productive upwelling and offshore river plume areas commonly reaching the 1-10 range and an additional order of magnitude greater in highly eutrophic and higher latitude sites. Overall, the global range of blue water, coastal, and estuarine phytoplankton chlorophyll is nearly 5 orders of magnitude (0.01 to 1000 µg/l, Figure 3). The relative impact of chl *a* and accessory pigments on water column optics is thus highly variable and renders problematic the development of a single, robust algorithm to estimate pigment content by remote sensing.

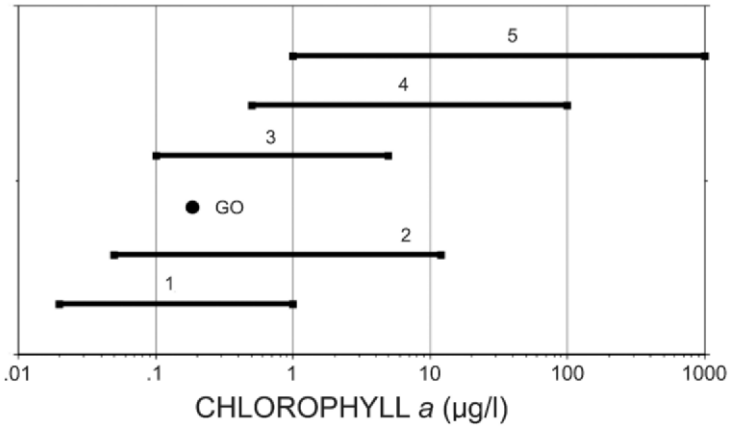

Figure 3. General ranges of chlorophyll a concentrations (mg/l = µg/l) for different ocean and coastal provinces: 1 - Sargasso Sea, Equatorial Pacific, Caribbean, 2 - California Current, 3 - Estuaries and Coastal Waters, 4 - North Atlantic, 5 - harmful algal blooms (Munday and Zubkoff, 1981; Carder and Steward, 1985; Kahru and Mitchell, 1998). GO = global ocean average of 0.19 (from Antoine et al., 1996).

Control of chl *a* levels and phytoplankton production are complex phenomena involving the interactions of physical, chemical, and biological processes (Jumars, 1993). Chlorophyll levels are generally controlled by nutrient and light availability, ratios of limiting resources, water column residence times and structural stability, water temperatures, and grazing pressure. Estuaries and other coastal embayments often have greater chlorophyll concentrations than adjacent offshore areas. However, offshore upwelling and plume activity can generate elevated pigment levels and increase spatial heterogeneity. Estuarine zones commonly have complex spatial patterns of biogeochemical constituents related to wind and tidal driven circulation patterns, longitudinal mixing gradients and point source inputs, and anthropogenic disturbances (Jassby et al., 1997). These spatial variability patterns are a major challenge in the design of estuarine sampling strategies.

In Georgia river transects extending from nontidal river reaches to offshore, we found a consistent pattern of increased chlorophyll within the estuarine mixing zone compared to upriver and offshore stations (Figure 4; also see Schalles et al., 1998a; Alberts et al., 2004). In these Georgia habitats, the mid and lower salinity reaches of the estuaries often have upper single to double digit chlorophyll levels and offshore shelf areas are typically low to mid single digit levels. The lower reaches of these estuaries also have elevated total and inorganic seston levels (Alberts et al., 2004). Upstream nutrient inputs, increased water residence times, nutrient sequestration and recycling in tidal wetlands and benthos, complex circulation patterns, ebb tide export of littoral zone phytoplankton and epibenthic algae, and wind-driven sediment resuspension all contribute to greater productivity and biomass in many estuaries.

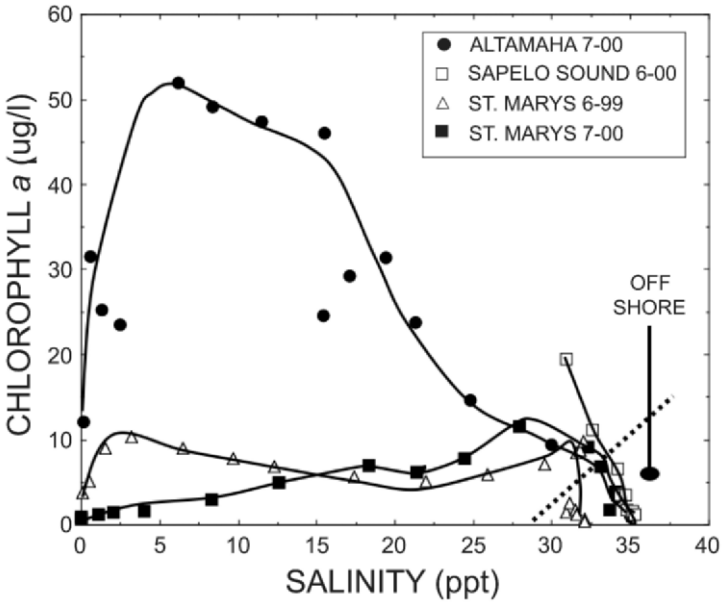

Figure 4. Chlorophyll *a* (not corrected for phaeophytin) versus salinity patterns for three Georgia estuaries and adjacent offshore areas (dashed, slanted line demarcates offshore stations). Data from two transects are shown for the St. Marys River.

3. Inherent Optical Properties and Constituent Absorption and Scattering

Chlorophyll remote sensing is based on detectable patterns within apparent optical properties. Radiative transfer equations describe the interactions between the inherent optical properties, or IOPs (e.g. absorption and scattering coefficients) and apparent optical properties, or AOPs (e.g. downwelling scalar irradiance attenuation, irradiance reflectance) for a given time, location, and atmospheric condition. Barnard et al. (1998) used a pair of *in situ* profiling ac-9 transmissometers (9 wavelengths; WET Labs, Inc), one with prefiltration of seawater, to operationally differentiate IOPs in a wide variety of ocean, coastal, and estuarine conditions. Their IOP data for 488 nm are summarized in Figure 5. The IOP measurements typically varied by one to two orders of magnitude for a particular location and cruise, and the total range for individual IOPs was two to four orders of magnitude. Not surprising, the equatorial Pacific had the lowest overall absorption and scattering values and the two estuarine sites (Chesapeake Bay and East Sound, Washington) had the greatest values. The coastal Case 2 waters generally had component absorption and scattering values above 0.1 m^{-1} whereas the clearest Case 1 waters had values between 0.0001 and 0.1. Considerable coherence existed between measurements at different wavelengths.

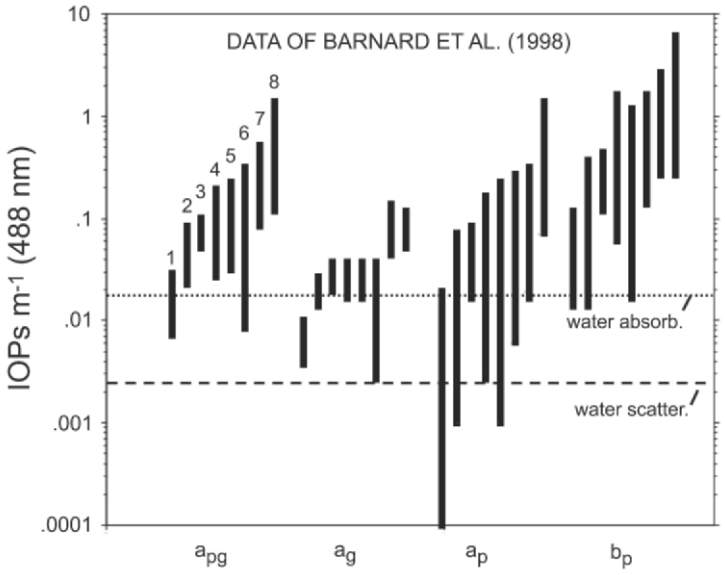

Figure 5. Summary of the ranges of inherent optical properties at 488 nm (from Table 2 in Barnard et al., 1998) for eight cruises and greater than 1900 measurements from 77 total profiles. Notation for coefficients: a_{pg} = total absorption (excluding water absorption), a_g = chromophoric dissolved absorption, a_p = particulate absorption, b_p = particulate scattering. Numbers above bars (shown only for a_{pg} values) refer to cruises: 1 - Equatorial Pacific, 2 and 5 - Gulf of California, 3 and 4 - North Atlantic Shelf, 6 - Near coastal California, 7 - Chesapeake Bay, 8 - East Sound, Washington. Absorption and scattering values for pure seawater (Mobley, 1994) are placed as reference lines.

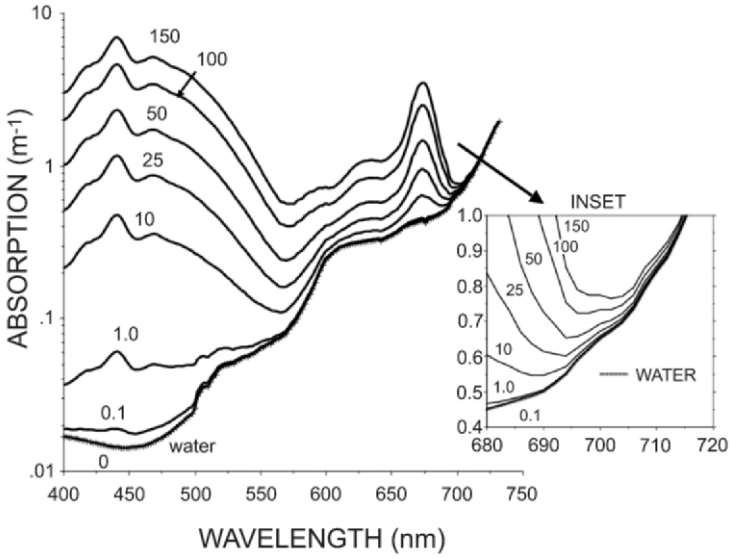

Figure 6. Semi-logarithmic plot of combined absorption coefficients for water and a model phytoplankton pigment suite at different concentrations of chlorophyll *a*. Pigment coefficients are based on the product of pigment specific absorption coefficients (m^2 mg^{-1}) and the average concentrations of chlorophyll and carotenoid fractions (μg/l) measured on four Sargasso Sea cruises (in Bidigare et al., – see text). Water absorption coefficients for pure seawater are from Smith and Baker, 1991. The inset shows the critical region near 700 nm where a localized peak of phytoplankton reflectance occurs at the point of minimum combined absorption by water and pigment.

The interaction of pigment and water absorption (Figure 6) provides important insights for the interpretation of minima and inflexion points in spectral reflectance curves. The pigment absorption data in Figure 6 assume the following fractional proportions, referenced to chl *a* (average values are from four Sargasso Sea cruises presented in Table 2 in Bidigare et al., 1990): chl *b* = 0.266, chl *c* = 0.083, photosynthetic carotenoids = 0.450, and photoprotective pigments = 0.236. At chl *a* = 0.1 and 1.0 μg/l, total pigment absorption adds comparatively little to water absorption above 500 nm. Hence, algorithms utilizing information from the red absorption peak will have little sensitivity for chl *a* values below 1, whereas pigment absorption has maximal separation from water in the Soret band region near 440 nm (Figure 6). A distinctive absorption minimum, corresponding to the green reflectance peak, occurs near 565 nm in this example. Note that a second local minimum occurs in the region of 680 - 710 nm (see inset in Figure 6). This minimum represents a region between stronger pigment absorption in the red Q band at adjacent lower wavelengths and much stronger water absorption at adjacent higher wavelengths. Note also that the wavelength position of this minimum shifts to higher wavelengths with higher pigment concentrations. This behavior has important bearing on the behavior of a corresponding peak in reflectance spectra in this same region produced by a combination of pigment fluorescence and phytoplankton cell scattering. Although many authors attribute this peak to chl *a* fluorescence (see discussion below), the wavelength position of chl *a*

fluorescence should not shift notably with increasing pigment concentration, compared to the shift in the absorption minima.

Scattering of light by water and its constituents is a particularly complex phenomenon involving both reflectance and refraction of molecules and particulate matter (Kirk, 1994). Pure water and pure seawater (water and dissolved inorganic ions at a salinity of about 35 parts per thousand) have a strong, inverse relationship between wavelength and scatterance, with a wavelength dependence of $\lambda^{-4.32}$ (Morel, 1974). However, seawater ions are responsible for an increase in the random fluctuations of the number of molecules per volume of water, and seawater consequently has about 30% greater scattering (b_w) than does pure water. The angular distribution of scattering is dependent on particle size and wavelength. The shape of the scattering angle to volume scattering function in strongly inverse and the slope of this relationship appears relatively constant across different water types and turbidities (Mobley, 1994). At a temperature of 20^{o}C, water has a refractive index of 1.3433 at 400 nm and an index of 1.3289 at 768 nm. The refractive indices of inorganic particles (~1.15-1.20) are greater than those of organic matter (~1.03-1.04) (Jerlov, 1976). Furthermore, algal cells with hard outer walls and soft, watery protoplasm may scatter more light than predicted based on the separate refractive indices of the two materials (Zaneveld et al., 1974). The complex refraction and external and internal reflectances of algal cells is apparently responsible for the larger scattering values per unit weight observed with phytoplankton compared to tripton (Dekker, 1993). In general, the scattering coefficients of turbid waters have less wavelength sensitivity than in pure water. An inverse relationship between wavelength and scattering also occurs in turbid waters, and spectral dependency (slope) is generally stronger for algae than for inorganic particles (Dekker, 1993).

Increased scattering results in an increase in the effective path lengths that light travels within water columns (Kirk, 1994). Increased scattering shifts the angular distributions of light and increases the probability that photons will re-emerge from the water column as a reflectance signal. One important consequence of increased scattering is a decrease in optical depth and reduction in the photic zone volume (Bukata et al., 1995). Also, in a water column with more diffuse light and longer effective path lengths, the probability of photon absorption increases. As discussed below, increasing particle densities thus amplify pigment absorption related differences in the magnitudes of the peak and trough reflectance used in chl *a* algorithms. In more productive and turbid waters, the "black pixel" assumption of negligible photon emergence at infrared wavelengths becomes invalid due to increased scattering and can lead to significant errors in chlorophyll retrieval (Siegel et al., 2000). Relaxation of this assumption can significantly improve chl *a* retrieval from satellite imagery in waters with chl $a > 2$ μg/l. Indeed, the NIR spectral region often yields the best remote sensing relationships between seston concentrations and water reflectance (Schiebe et al., 1992; Kirk, 1994).

4. Instrumentation, Calibration, and Biases

The dynamic range of radiometric measurement, spectral resolution, and number and position of bands are critical sensor design elements that greatly affect the operational abilities of instruments to detect chl *a* signals in different optical regimes. Field spectroradiometers and aircraft and satellite sensors have wide variations in the number of channels (bands) and bandwidths, foreoptics and viewing geometries, and

detector array configurations. Chl *a* absorption of red light occurs in a rather narrow band. Optimal detection of the chlorophyll red absorption peak in laboratory spectrophotometers requires a spectral bandwidth of 2 nm or less (Rowan, 1989). The blue, Soret band of chl *a* has a comparably narrow absorption peak. Broader bandwidth not only reduces the ability to resolve these peaks, but also allows greater overlap with the absorption regions of accessory chlorophylls (especially chl *b*) and other pigments. These wavelength resolution issues may have similar importance in measurements with field radiometers. However, signal-to-noise constraints in field spectroradiometers and remote platform sensors may necessitate broader bandwidth (Dekker, 1993).

Wavelength selection for pigment detection is affected by a well known wavelength shift (roughly 5-10 nm) for the wavelength of maximum pigment absorption in extracted versus *in vivo* conditions. For example, chl *a* and *b* in 90% acetone have maximum absorption values at 664 nm and 647 nm (consensus averages from Rowan, 1989) whereas Bidigare et al. (1990) estimated the maximum red absorption *in vivo* at the longer wavelengths of 674 nm and 652 nm (see Figure 1). Also, the wavelengths of maximum red absorption for chl *a* can vary by about 5 nm, depending on the extractant and pH conditions (Rowan, 1989). Chl *a* has a prominent left "shoulder" of absorption associated with the blue, Soret band and a secondary red absorption peak broadly centered at 628 nm (Figure 1). Ratios of *in vivo*, weight specific absorption coefficients for the blue and red primary peaks and the blue and red secondary peaks are about 1.3 and 4.95, respectively (Bidigare et al., 1990). Global ocean comparisons reveal that chl *a*, total carotenoids, chl *c* and chl *b* account for about 47%, 43%, 8%, and 4% of total phytoplankton pigment, although a range of 35% to 53% for chl *a* was reported for different bio-optical provinces (Aiken et al., 1995).

Maintaining proper instrument calibration is an important but sometimes challenging issue. Wavelength to channel registration and radiometric energy calibration may not be stable over time (Evans and Gordon, 1994; Starks et al., 1995). Instruments should be checked periodically for gradual drift or erratic changes that may be related to operating temperature or to degradation or damage to the optical components or their light path alignments. Wavelength specific lasers, emission lines from lamps, and narrow pass filters are commonly used to establish a regression fit between known wavelengths and the instrument channels with maximum response to these signals (Starks et al., 1995). Radiometric responses of individual channels are calibrated against well characterized lamp emission responses. Proper radiometric calibration can be more difficult when foreoptics and/or fiber optic guides deliver light to the optical slit entrance of the instrument. Researchers performing close range measurements with spectroradiometers usually convert their water spectra measurements to fractional or percent reflectance, a normalization procedure in which upwelling and downwelling estimates are ratioed for each channel of an instrument or pair of instruments.

Bottom substrate reflectance contributes to and can cause bias in the composite upwelling irrandiance and reflectance signals in optically shallow waters (Akleson and Klemas, 1986; Maritorena et al., 1994; Lee et al., 1998; Odhe and Sigel, 2001; Albert and Mobley, 2003), and may interfere with interpretation of water column signals and chlorophyll retrieval. Rundquist et al. (1995) measured reflectance from black and white panels suspended at 10 cm depth intervals between 2 and 82 cm during dilution of an algal bloom in an outdoor tank mesocosm. With the black panel at 82 cm, a ratio of the NIR peak reflectance to chlorophyll absorption band reflectance near 674 nm (Mittenzwey et al., 1992) had a linear relationship to chl *a* over a range of 30 to 336 μg/l (r^2 = -0.98, n = 15). The white panel had an amplifying effect on spectral

reflectance, and also amplified the differences between spectral peaks and troughs in a manner similar to suspended clay additions (see below). In the experiment, the NIR/red ratio increased about 40-50% with a white, reflective bottom and optically shallow conditions. Because of wavelength dependent light attenuation patterns, signal return from bottom substrates may occur at some wavelengths and not others. In general, chl *a* indices at higher wavelengths will be less biased than indices using lower wavelengths because of greatly increased light attenuation by water at red and especially NIR wavelengths. Boss and Zaneveld (2003) demonstrated that interactions of bottom substrate and overlaying water may strongly affect the IOPs of the water column, with greatest effects on absorption and/or scattering in near bottom waters.

Water surface effects may also cause substantial changes in light fields and remote sensing reflectance (Kirk, 1994). Light reflectance at the air/water interface is strongly affected by incident solar angle and by wave activity. Workers generally seek to avoid direct solar beam reflectance sun glint (glitter) effects by: 1) reducing the instrument's field of view; 2) directing the view angle away from sun's incident angle; and 3) restricting the time of day for measurements to avoid high or extremely low zenith angles. During strong winds, wave turbulence can lead to surface foam and entrained air bubbles in the upper several meters of water. Bubble backscattering has minimal effect on downwelling irradiance, but can increase upwelling radiance and reflectance five fold in the upper several meters (Mobley, 1994).

5. Examples of Water Reflectance Spectra

A series of water reflectance spectra measured close range by my research group using a pair of USB2000 spectroradiometers (Ocean Optics, Inc.) are compared in Figure 7. The spectra were selected to illustrate water color reflectance signals in a broad range of water types. The ranges of OACs at these locations were quite diverse (C = chlorophyll *a*, range = 0.03 - 272 μg/l; S = total seston - i.e. suspended solids, range = 1 - 106 mg/l dry weight; A = CDOM absorption at 440 nm, range = 0.18 - 12.3 m^{-1}). The chl *a* values were not corrected for phaeophytins, and thus represent a combined pigment set. These measurements represent a four orders of magnitude range in chl *a*. Reflectance spectra were measured as downwelling solar irradiance in air and upward radiance (25° field of view) at nadir angle just below the surface, and were computed at each wavelength as the ratio of the upward radiance just below the surface, $L_u(0-)$, to the downward irradiance measured in air, E_d (0+).

The Caribbean spectra, measured in deep water (about 600 m) off the north coast of Roatan Island, Honduras demonstrates an ultraoligotrophic condition (chl *a* = 0.03 μg/l) with high blue reflectance (about 8.5% at 400 nm), strongly decreased reflectance with increasing wavelength, and virtually no measurable signal above 600 nm. This lack of return signal corresponds to the sharp increase in water absorption coefficients (0.08 m^{-1} at 580 nm versus 0.3 m^{-1} at 620 nm; see Figure 6). Conversely, the scattering coefficient for water is only 0.0014 m^{-1} at 600 nm as compared to 0.0076 m^{-1} at 400 nm (Smith and Baker, 1981). Water color at this station was blue-violet. The spectra resembled modeled and observed blue water spectra in the Sargasso Sea and Crater Lake, Oregon (Morel and Prieur, 1977) and exemplifies locations where the clear seawater end member dominates reflectance. The tropical lagoon spectra, also measured at Roatan Island, represented a water condition with 20 times greater chl *a*, and 4-5 times greater seston and CDOM concentrations. A broad green maximum with

peak reflectance between 530 and 570 nm was present. Blue reflectance was sharply reduced compared to the offshore station. Reflectance was detectable to about 725 nm.

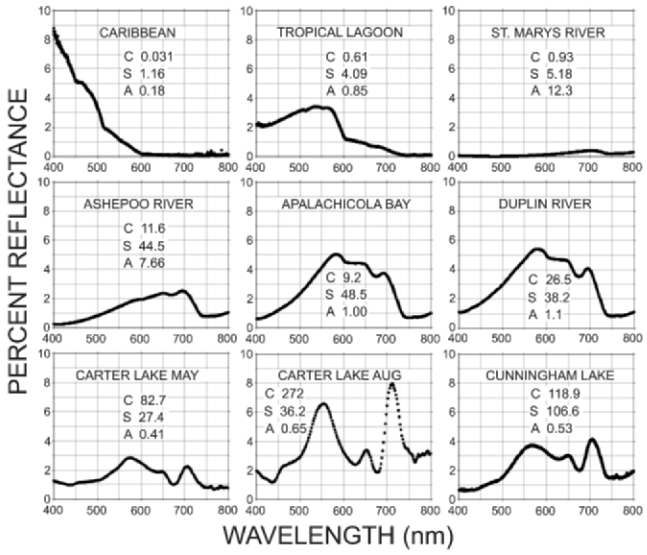

Figure 7. Water reflectance spectra measured by the author at various coastal, estuarine, and inland locations representing a broad range of optically active constituents. Caribbean and tropical lagoon sites - deep offshore waters and Man-O-War lagoon at Roatan Island, Honduras, C.A.. All other sites in the U.S.A.: St. Marys River - upstream station on Georgia/Florida border; Ashepoo River - mid river station in coastal South Carolina; Apalachicola Bay - western Florida; Duplin River - a tidal river at Sapelo Island, Georgia; ; Carter Lake - Missouri River floodplain lake on Nebraska/Iowa border; Cunningham Lake - flood control and recreation reservoir in Omaha, Nebraska. Note: C = µg/l of chl *a*, not corrected for phaeophytin; S = mg/l of total seston; A = m^{-1} of CDOM absorption at 440 nm.

The St. Marys River, at the eastern border of Florida and Georgia, typically has very high CDOM levels (Alberts and Filip, 1994). Spectra were acquired at a river station during a period with an extremely high CDOM level (ABS_{440} nm = 12.3 m^{-1}), very low chl *a*, and moderate total seston. Reflectance was well below 1% (Figure 7). A subdued reflectance peak (about 0.45%) was centered near 700 nm and no green peak was present. In this spectrum CDOM absorption (see below) suppressed scattering return at all wavelengths, but most notably in the blue and green regions. The scattering return was largely due to ultrafine clay-detritus aggregates (~ 16 µm diameter) that occur in these coastal plain rivers (Carlough, 1994). This curve is a good example of CDOM end member dominance. The Ashepoo River in South Carolina also had high CDOM concentrations and much higher chlorophyll loads and total seston loads than the St. Marys River. This spectrum was measured at a station with ABS_{440} (a measure of CDOM concentration) of 7.66, chl *a* of 11.6 µg/l, and total seston of 44.5 mg/l and had maximum reflectance of about 2.5% from 650 to 700 nm, with a modest pigment absorption trough near 670 nm. Reflectance remained below 1% between 400 and 500 nm and increased to 1.5% at 550 nm. The particulate load created notable NIR

reflectance (about 1% between 735 and 800 nm) compared to the St. Marys River example (discussed below).

The Apalachicola Bay (Florida), and Duplin River (Sapelo Island, Georgia) spectra represent relatively turbid (total seston concentrations of 48.5 and 38.2 mg/l), moderately productive ecosystems (chl *a* concentrations of 9.2 and 26.5 µg/l) with about an order of magnitude lower CDOM than the previous two river examples (Figure 7). Both spectra had maximum reflectance (about 5% and 5.5%) near 580 nm and a similar NIR reflectance (about 1%) to the Ashepoo River spectrum. In both spectra, an inflexion near 600 nm and plateau extending from about 600 to 650 nm were caused by the interplay of seston scattering and the sharply higher water absorption in this spectral region (see Figure 6). In contrast to the St. Marys and Ashepoo examples, these spectra have noticeably larger chl *a* absorption features near 670 nm, with the larger chlorophyll load in the Duplin example causing a larger red trough feature and a more distinctive localized maximum near 690 nm. These local peaks represent the spectral position of minimum combined pigment and water absorption (Figure 6, see inset). Blue reflectance, although very low compared to the Caribbean blue water example, was greater than the St. Marys and Ashepoo examples. The higher blue and green reflectances in the Apalachicola and Duplin examples were presumably due to the much lower CDOM levels.

The final three example spectra in Figure 7 represent highly eutrophic sites in Nebraska. Carter Lake is a hypereutrophic lake on the Missouri River floodplain near Omaha (Schalles et al., 1998b; Schalles and Yacobi, 2000). A spring (May) example, during a bloom of the diatom *Synedra* sp. with a chl *a* concentration of 82.7 µg/l, had two spectral maxima near 574 nm and 702 nm, and relatively low (about 1%) and level reflectance between 400 and 500 nm (Figure 7). The upward wavelength shift of the NIR maximum (peak) above 700 nm is consistent with the shift in the absorption minimum with increased chl *a* (see inset, Figure 6). A pronounced chl *a* minimum was centered at 673 nm, with a prominent shoulder between 625 and 650 nm produced by both chls *a* and *c* (see Figure 1).

The Carter Lake August spectrum reveals extreme dominance by the filamentous cyanobacterium *Anabaena* sp., with a chl *a* concentration of 272 µg/l. The cyanobacterial pigment phycocyanin produced a distinctive reflectance minimum, centered at 625 nm (Dekker et al, 1996; Schalles and Yacobi, 2000). Phycocyanin concentration was estimated at 450 µg/l, yet the magnitude of its absorption trough was not as pronounced as the chl *a* trough. Phycocyanin absorption per unit of pigment is only 20% of the absorption per unit of chl *a* (Rowan, 1989). The position of the green peak (reflectance about 6.6%) was reduced by 20 nm, to 553 nm, compared to the May spectra (Figure 7). Carotenoid absorption (see Figure 1) "erodes" the left shoulder of the green peak and shifts its maximum to higher wavelengths. In response to the overall bloom dynamics, total carotenoids doubled from about 45 to 90 µg/l between May and August (Schalles and Yacobi, 2000). However, in the cyanobacteria bloom period phycocyanin has an even more dominant optical effect by eroding the right shoulder and shifting the green peak to lower wavelengths. A significant inverse correlation existed between phycocyanin concentration and green peak position ($r = -0.912$) in Carter Lake and resulted in regular, seasonal patterns of green peak position shifts during four years of observations (Schalles and Yacobi, 2000). Note, also, that the simultaneous erosions of the left and right shoulders of the green peak by carotenoids and phyocynanin may supress the overall height of this peak. At this high level of chl *a*, the blue, Soret band absorption (Figures 1 and 6) produced a distinctive minimum near 440 nm and the red absorption induced minimum (about 2% at 675 nm) was sharply

lower than the adjacent NIR maximum (8% at 712 nm). The upward spectral shift of the NIR peak with increased chl *a* has been widely observed (Gitelson, 1992; Gitelson et al., 1999) and is explained by an upward shift in the position of minimum combined absorption by pigment and water with increased chlorophyll concentrations (Figure 6). The comparative heights of the NIR peak and the chl *a* red trough are used in several chlorophyll algorithms for Case 2 waters (Dekker, 1993; Ammenberg, 2000; Gitelson et al., 2000, Gons et al., 2002; see below).

Cunningham Lake is a eutrophic, clay-rich, turbid reservoir near Omaha within an agricultural watershed. A late summer example with high chl *a* and total seston concentrations of 118.9 μg/l and 106.6 mg/l is shown in the last panel of Figure 7. Phytoplankton composition was quite diverse, with abundant cynaobacteria and dinoflagellates as well as diatoms and chlorophytes. Green and NIR maxima occurred at wavelengths similar to the May Carter Lake example, but with higher reflectance. Reflectance at the NIR peak exceeded green peak reflectance (4.1% versus 3.7%) in contrast to green peak dominance in the first Carter Lake example, with an overall pattern more similar to the August spectrum. The dinoflagellate carotenoid pigment peridinin has significant activity in the mid-500 nm region and suppresses the green peak magnitude (Gitelson et al., 1999). Additionally, combined pigment and water absorption in the green peak region is more affected by increased pigment loads than the NIR peak position (Figure 6).

6. Tank Mesocosm Studies

6.1 PHYTOPLANKTON DENSITY AND COMPOSITION AND THEIR EFFECTS ON REFLECTANCE

Experiments with manipulations of OACs in indoor and outdoor tanks (ex. Krijgsman, 1994; Schalles et al., 1997; Schalles et al., 2001) have provided calibration data for pigment estimation algorithms, empirical evidence for interactions between phytoplankton and other constituents, and tests of bio-optical models. The results of spectral reflectance measurements from a tank mesocosm experiment at the former National Agricultural Water Quality Laboratory (USDA-Agricultural Research Service) in Durant, Oklahoma, illustrate the optical interactions of a graded series of phytoplankton densities with water. In this experiment (Figure 8, from Schalles et al., 1997), a mixed culture of green algae was grown to bloom state in an 80 m^3 outdoor tank. The tank depth was 3.2 m. *Chlorella* sp. accounted for 92% of cell density and *Scenedesmus* sp. for an additional 7% after bloom development. The upper 80% of the culture tank's water was transferred to a separate tank (dilution tank) to minimize settled detrital particles and brought to full volume with clear water. In the experiment, the bloom water was sequentially diluted with clear water from two additional tanks and volume was balanced by pumping the phytoplankton tank water to a clearwater, enrichment tank. Complete tank mixing was accomplished in 15-20 minutes with a pair of pumps drawing water from the bottom center, which was reinjected tangentially at the tank wall just below surface and at mid depth. For load balance, the enrichment tank was allowed to overflow to a drain. In this manner, phytoplankton cell densities were manipulated in a graded manner, achieving a chl *a* range of 0.4 - 62 μg/l. Initial cell density in the bloom water tank prior to dilution was 3.2 x 10^5 cells/ml.

A hinge point near 510 nm was observed in the resultant family of spectra (Figure 8). At wavelengths below 510 nm, reflectance decreased with increasing cell density - direct

evidence that pigment absorption was dominant. Note that peak reflectance was about 1.5% at 400 nm, which is much lower than the 8.8% value for the Caribbean station in Figure 7 in the absence of deep water scattering. The chl *a* concentration was more than an order of magnitude greater in the tank compared to the Caribbean blue water example, and the black bottom of this tank, at a depth of 3.2 m, was visible in the clear water tank. At all wavelengths above 510 nm, reflectance increased with increasing cell density, although the magnitude of increase varied as a function of wavelength dependent absorption behaviors. Bukata et al. (1995) demonstrated similar results when their multi-component optical model for natural waters was parameterized with no CDOM present and no, or very low, amounts of suspended matter (tripton). With no CDOM or tripton present, their spectral pivot point occurred at 497 nm, the wavelength for which the ratio of $(b_b)_{chl} / a_{chl} = (b_b)_w / a_w$ (where b_b = backscatter, a = absorption, chl = an average phytoplankton condition, and w = pure water). Their modeled hinge point shifted to 528 nm with the addition of 0.1 mg/l tripton and to much higher wavelengths with higher tripton concentrations. Their model is also sensitive to the optical characteristics of the phytoplankton parameterization.

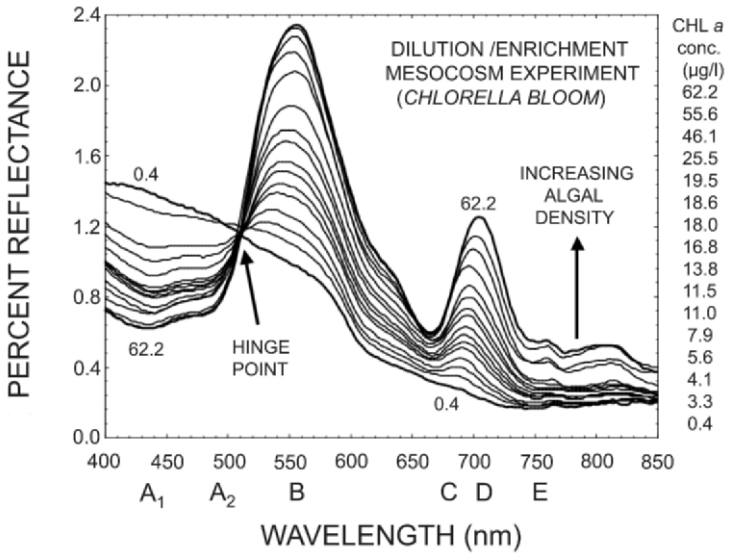

Figure 8. Graded series of reflectance spectra for different chl *a* levels (0.4 to 62.2 µg/l) for a dilution/enrichment scheme experiment (Schalles et al., 1997) involving two, 3.2 m deep mesocosm tanks. Note: letters along the X axis designate wavelength regions used for many chlorophyll algorithms (see text for explanation).

In the experiment in Figure 8, green reflectance increased from approximately 1 to nearly 2.4% as cell density increased. A noticeable peak near 550 nm became evident at chl *a* concentrations above 4 µg/l. The wavelength position of the green peak increased about 6 nm with increasing cell densities, presumably from erosion of the left shoulder of the peak by carotenoid absorption. A slight shoulder developed at about 620 nm, in the region of the secondary red peak of chl *b* (Figure 1). A well defined minimum (trough), centered near 670 nm and associated with the Q band of chl *a*, developed with

increasing cell density (Figures 8, 9), as did the adjacent reflectance maximum (peak) near 700 nm. As seen in Figure 9, the position of maximum reflectance for this peak increased about 20 nm (from 685 to 705 nm), coincident with increasing pigment concentration and a shift in the position of minimum combined absorption by pigment and water (Figure 6).

A key observation apparent in Figures 8 and 9 is the appearance and intensification of peaks versus troughs with increasing cell densities. Increased scattering occurs at all wavelengths with increased cell densities. This scattering decrease with increasing wavelength is essentially monotonic (Mobley, 1994), and thus cannot account for the peaks and troughs coinciding with phytoplankton communities of different densities. Reflectance "troughs" develop at spectral regions of stronger pigment and/or water absorption and the "peaks" at regions of absorption minima (Figure 6). Therefore, phytoplankton density controls reflectance at these peak and trough positions, and are the primary signals available for remote sensing detection of chl *a* and, potentially, other pigments.

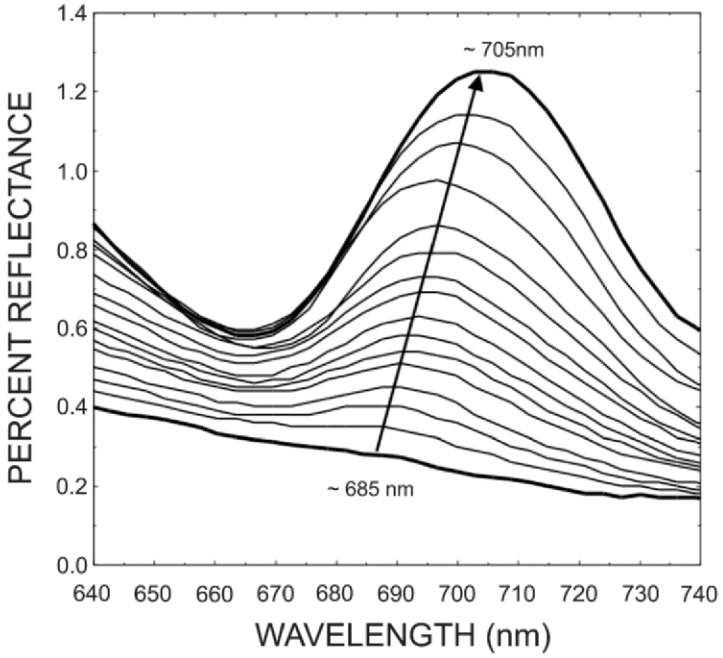

Figure 9. Magnification of the spectral region 640 to 740 nm from Figure 8, illustrating the increase in magnitude and the shift in wavelength position (arrow) of the NIR peak near 700 nm in a series of reflectance spectra with chl *a* levels of 0.4 to 62.2 µg/l.

The graded series of reflectance spectra (Figures 8 and 9) illustrate the basis for the predictive algorithms used in optical remote sensing of chl *a*. In ocean color schemes for Case 1 waters, bands in the blue and green regions (Figure 8, points A_1 - 443 nm, A_2 - 490 and/or 510 nm, and B - 550 or 555 nm) and others are commonly used (Gordon and Morel, 1983; O'Reilly et al., 1998). Oligotrophic, blue water conditions have an inverse relationship of reflectance and wavelength (Figure 7) due to increasing

absorption by water with increasing wavelength (Figure 6) and blue dominated, wavelength specific scattering efficiencies (Smith and Baker, 1981). Modest increases in phytoplankton density, accompanied by increased pigment absorption (Figure 8), result in strongly decreased blue reflectance (tropical lagoon example in Figure 7 and point A_1 in Figure 8), while scattering outcompetes absorption in the green peak region and results in increasing reflectance (points B_1 and B_2 in Figure 8). The ratio of 443 to 555 nm (Figure 10) is strongly and inversely correlated and has been used to estimate chl *a*. The relationship, however, is nonlinear and becomes increasingly less sensitive with increasing pigment (especially above 10 µg/l).

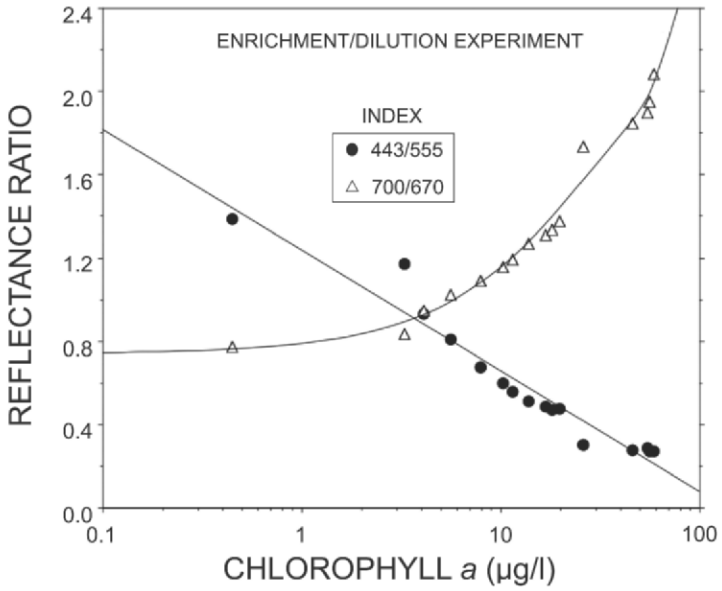

Figure 10. Comparison of two common chlorophyll algorithms: (1) ratio of 453/555 nm for Case 1 waters and (2) ratio of 700/670 nm for turbid and/or eutrophic Case 2 waters. Data are from the mesocosm dilution and enrichment experiment in Figures 8 and 9.

Algorithms based on Q band, red absorption and the NIR reflectance peak feature are favored in situations with high chl *a* and/or Case 2 optical conditions (Dekker et al., 1996; Gower et al., 1999; Ammenberg, 2000; Gitelson et al., 2000; Gons et al., 2002). A band ratio using the NIR peak near 700 nm and the red Q band may largely isolate the chl *a* signal from other pigment and CDOM absorption activity. The NIR feature builds much more rapidly than the Q band region with increasing cell densities (Figures 8 and 9), producing an exploitable response. A ratio of 700 nm to 670 nm (Gitelson et al., 2000), applied to our tank mesocosm data, produced a strong relationship to chl *a*, with good sensitivity above 10 µg/l (Figure 10).

Different phytoplankton taxa often have differentiable colors, i.e. are members of the "green algae", golden brown algae", etc., with these variations clearly related to spectral differences in absorption by accessory pigments (Sathyendranath et al., 1987; Rowan, 1989; Richardson, 1996). Thus ecologically different oceanic provinces, with differing proportions of dominant phytoplankton groups, may have differing absorption

and scattering properties that affect remote sensing bands and the band ratios for chlorophyll estimates. These differing bio-optical properties may partially explain the poorer performance of ocean color chlorophyll algorithms in waters at polar latitudes (Sathyendranath et al., 2001). In Figure 11 the reflectance characteristics of phytoplankton from four taxomic divisions are compared, with each containing chl *a* concentrations of about 60 μg/l. In this figure, two spectra were measured in our Durant, Oklahoma mesocosm experiments (*Navicula* and *Chlorella*) and two were measured from lakes with nearly monotypic assemblages (*Anabaena* and *Peridinium*). *Navicula* is a pinnate diatom, *Chlorella* is a small, spherical non-filamentous chlorophyte, *Anabaena* is a filamentous cynabacterium, and *Peridinium* is a large, oval dinoflagellate. Large quantitative differences exist in the four spectra. Higher reflectivity of the silica frustule in *Navicula* probably accounts for the overall stronger reflectance, including the NIR region beyond the region of pigment activity. In addition to prominent Soret and Q band chl *a* minima, the diatom spectrum had conspicuous shoulders near 480 nm and 630 nm, coincident with carotenoid and chl *c* absorption maxima (Figure 1). The *Anabaena* spectrum was measured in Carter Lake (compare to Carter Lake examples in Figure 7) in early July, 1996, as the bloom was developing. The NIR peak was nearly as large as the green peak, with the green peak position about 15 nm to the left of the diatom and dinoflagellate positions. Additionally, a significant phycocyanin trough (620 nm) was present. The *Peridinium* curve, from Lake Kinneret, Israel (Gitelson et al., 1999), had a narrower green peak, probably due to strong accessory pigment activity on each side. This curve was taken from a series of spectra, acquired on the same date in different bloom densities, which demonstrated that green peak reflectance decreased with chlorophyll concentrations above 10 μg/l (Gitelson et al., 1999). In contrast, the NIR peak increased with increasing cell and chl *a* levels. Green peak suppression was probably due to the broad absorption profile of peridinin (Richardson, 1996), a pigment unique to dinoflagellates. Peridinin also suppresses the green reflectance peak in zooxanthellae symbionts of corals (Meyers et al., 1999). The *Chlorella* spectrum, taken from the tank experiment discussed above (Figure 8), had the lowest overall reflectance, and a relatively broad and symmetrical green peak.

Using the data shown in Figure 11, the Case 1 water, blue to green ratio for chl *a* (443 nm to 555 nm) was computed for each taxon's spectrum, and compared to the Case 2 water ratio of 670 nm to 700 nm (Figure 12). Note that the denominator and numerator of the Case 2 ratio is reversed from the last case discussed (Figure 10) to allow a more direct comparison with the Case 1 ratio. In this comparison, the ocean color ratio was more variable (coefficients of variation for the Case 1 and Case 2 ratios were 34.0% and 8.7%, respectively). The Case 2 band ratios (chl *a* estimate) using 670 and 700 nm were more consistent when applied to the four spectral data sets, compared to the Case 1 ratio (433 to 555). In the latter case, the ratio differed (for almost the same chl *a* concentration – see Figure 11) for all four taxa, and by almost a factor of 3 for *Chlorella* (62 μg/l chl *a*) vs. *Peridinium* (61 μg/l chl *a*). The higher variability in the spectral responses for the 443 to 555 ratio was likely due to the greater impact of accessory pigments, especially carotenoids, at these wavelengths.

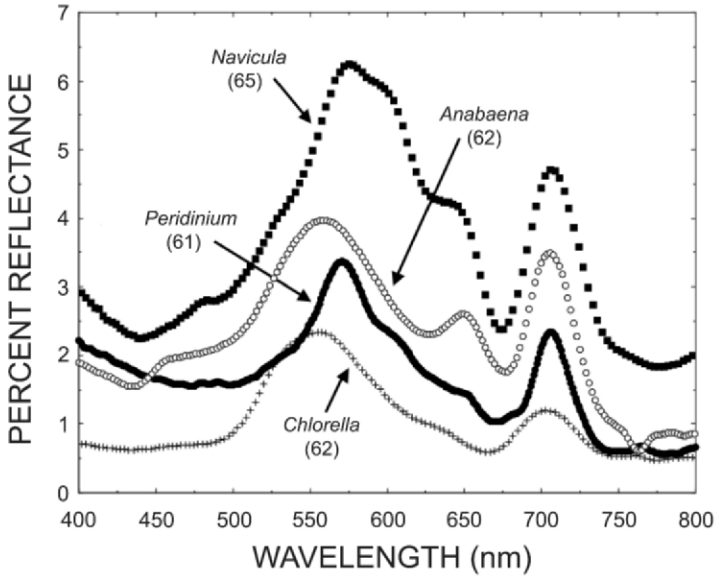

Figure 11. Comparison of reflectance spectra for algal taxa representing four different divisions. The measured spectra are examples for nearly identical chlorophyll concentration (chl *a* concentrations, in µg/l, are given in parentheses).

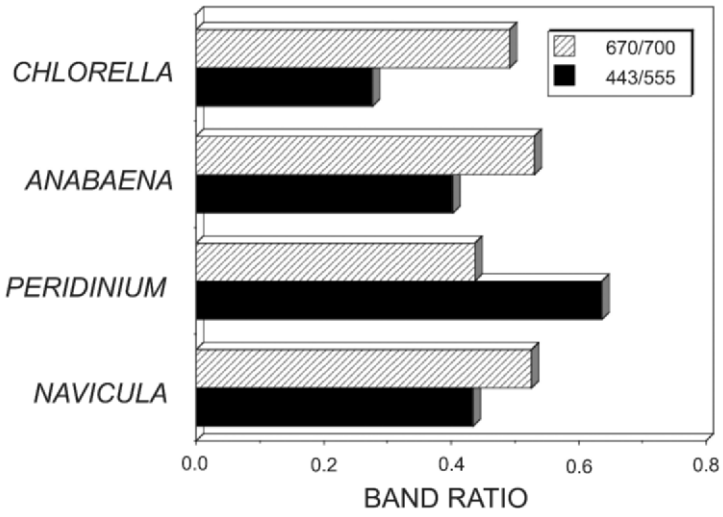

Figure 12. Comparison of two band ratios for chl *a* estimation for the reflectance spectra of four different algal taxa with nearly identical (measured) chl.*a* concentrations (see Figure 11).

6.2 CLAY SUSPENSIONS AND THEIR EFFECT ON REFLECTANCE

In general, inorganic tripton particles such as clays and carbonate minerals increase the albedo of water in a density dependent manner, due to strong scattering efficiency and comparatively low absorption. In contrast, absorption by organic tripton often resembles CDOM, with a strongly inverse correlation between wavelength and concentration (Dekker, 1993). In an experiment with the Durant, Oklahoma tank mescosms (Schalles et al., 1997), a suspension of white, kaolin clay was added in seven steps to clear water (Figure 13). Added clay concentrations ranged from 1.9 to 39.3 mg/l. Median particle size of the suspended clay was 0.79 μm (the 1st and 3rd quartiles were 0.66 and 0.95 μm). As the clay was added, the water turned a milky, white chalk color, with increased brightness. Reflectance increased in a stepwise manner, with the magnitude of reflectance above 500 nm inversely correlated with the spectral pattern of water absorption (Figure 6). The position of peak reflectance shifted from approximately 455 nm at 1.9 mg/l clay to 540 nm at 39.3 mg/l clay. At the highest clay level, peak reflectance was a remarkable 52.5%, notably higher than values reported for many other sediments in water (Curran and Novo, 1988; Han and Rundquist, 1994). Reflectance decreased sharply near 600 nm for all clay concentrations, in response to the sharp increase in water absorption (see Figure 6). Consistent with other findings, the reflectance response versus clay level was non-linear, becoming less sensitive at higher clay loads. Substantial NIR reflectance was found at the higher clay loads. For example, at 750 nm the reflectance was 2.7% and 7.1% for clay concentrations of 18.2 and 39.3 mg/l. The reflectances in this experiment probably approach the upper limits of scattering and return signals in water. Note, however, that clay turbid rivers and lakes may have tripton concentrations well in excess of 100 mg/l, and the highest concentrations may approach 1000 mg/l (Schiebe et al., 1992).

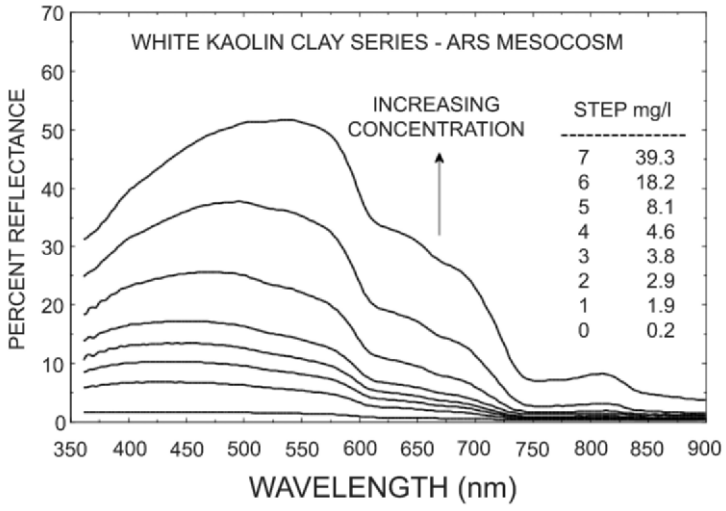

Figure 13. Effect of stepwise additions of white kaolin clay suspension on water reflectance. Clay was added to an 80 m^3 tank mesocosm with clear water (lowest curve), which had a seston concentration of 0.2 mg/l (the initial, pre-clay condition).

6.3 CLAY INTERACTIONS WITH PHYTOPLANKTON

In a separate mesocosm experiment, algal bloom water from a single, fertilized experimental tank was divided and added to two clean, empty 80 m^3 tanks (Schalles et al., 1997). One third of the bloom water was added to the first tank and two thirds to the second tank, taking care not to draw settled materials from the bottom of the fertilized culture tank. Clear, dechlorinated water was then used to fill the remaining volumes of the first and second experimental tanks. In this manner, algal suspensions were established with chl *a* concentrations of 31 and 57 µg/l. Both tanks had identical communities of algae, with the same age and size distributions, and the only difference in the starting conditions of the two ponds was cell density. In this experiment, nearly identical additions of the same white, kaolin clay used in the experiment shown in Figure 13 were made to both tanks in a stepwise manner. Clay was added in 6 increments, and the final increment achieved a concentration of 72 mg/l dry weight in both tanks.

Prior to clay additions, the tank with the higher chl *a* concentration had higher reflectance at all wavelengths, as seen in the bottom spectra with initial seston concentrations (Figure 14). The increase in reflectance with higher algal density was greater for both the green peak (4.4% in the high density versus 2.6% in the lower density tank) and NIR peak locations (2.7% versus 1.4%). Clay additions increased reflectance at all wavelengths, in a dose dependent manner. The white clay had little overall affect on the wavelength positions of peaks and troughs. Interestingly, at the higher clay levels, reflectance was greater in the lower algal density tank (a reversal from the starting condition with only phytoplankton present - see below for explanation).

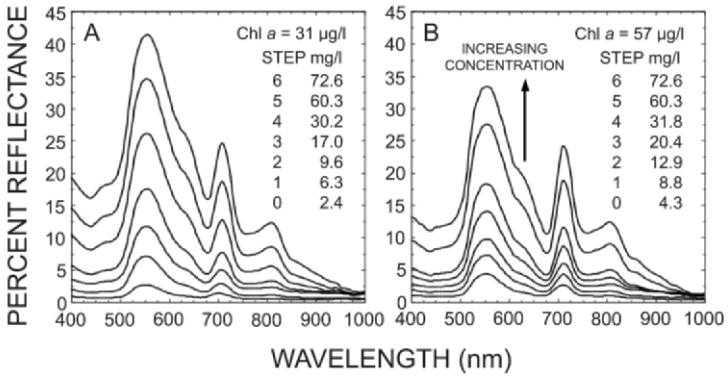

Figure 14. Effect of stepwise additions of white kaolin clay on water reflectance in replicate tank mesocosms with algal suspensions identical in taxonomic and particle size composition but differing in chl *a* concentrations (31 versus 57 µg/l). Note: lowest spectral curves (2.4 and 4.3 mg/l) are baseline conditions before clay additions.

The impact of clay additions on the 443 to 555 nm and 670 to 700 nm ratios for the data depicted in Figure 14 is summarized in Figure 15. The 443 to 555 ratio before clay additions was 0.252 in the low density tank and 0.198 in the high density tank. Overall, clay additions resulted in higher ratios. The ratio increased 55.2% in the low density

and 69.2% in the high density tanks. An increase in ratio values will result in underestimation of the chl *a* concentrations. Additionally, the ratios for the two tanks and chl *a* concentrations converged at intermediate clay levels, which is also problematic for algal quantification. These data agree with a model developed by Bowers et al. (1996) that predicted decreased slope and sensitivity in the chlorophyll relationship to the blue to green ratio with increasing mineral suspended solids (inorganic tripton).

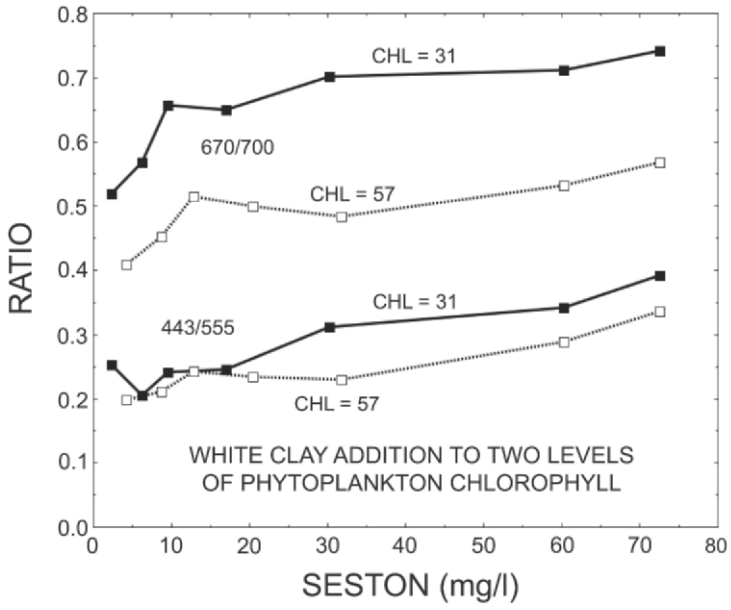

Figure 15. Effect of stepwise white clay additions to two tanks on two band ratios used for chl *a* estimation. The tanks contained identical algal communities at two different concentrations (31 versus 57 µg/l chl *a*; see Figure 14).

The 670 to 700 nm ratio in Figure 15 also increased with increased clay concentrations, which would again lead to underestimation of algal chlorophyll. However, the increases were more modest than those for the 443 to 555 ratio: 42.8% and 38.9% for the low and high density tanks, respectively. In contrast to the 443 to 555 ratio data, the response of the 670 to 700 ratio for the two algal concentrations was similar when clay was added in that the curves remained separate and mostly parallel (Figure 15).

At step four in the white clay addition to algae experiments (Figure 14), the total suspended solids (i.e. seston) concentrations were similar (17.0 mg/l and 20.4 mg/l) in the low and high algal density tanks. The 6th step in the clay addition to clear water experiment (Figure 13) resulted in a similar total suspended solids concentration (18.2 mg/l). The spectral curves for these three conditions (chl *a* = 0, 31, and 57 µg/l), each with similar total seston concentrations, are compared in Figure 16. Note the convergence of all three spectra at wavelengths above 725 nm, which corresponds to a region with virtually no algal pigment absorption (see Figures 1 and 6). The tank with the higher chl *a* (57 µg/l) had the lowest reflectance in the active pigment region, while

reflectance in the region of pigment absorption was about 25-30% higher in the low algal concentration tank (Figure 16). In contrast, the tank with no algae had substantially higher reflectance, particularly in the spectral regions corresponding to the greatest overall pigment activity (see Figure 6). At these pigment concentrations, pigment absorption is nearly two orders of magnitude greater than water absorption at wavelengths below about 500 nm. This disparity decreases rapidly with increasing wavelength (Figures 6, 16). The comparability of scattering activity in the three tanks was confirmed by the close agreement in reflectance values above 725 nm (Figure 16).

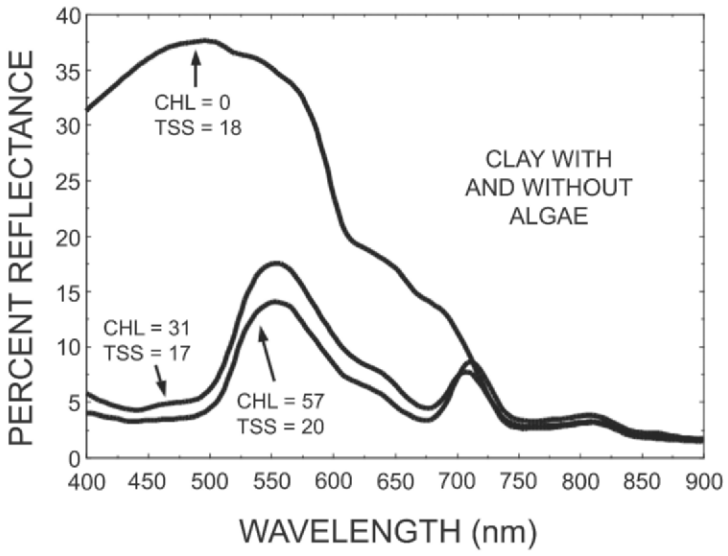

Figure 16. Comparison of three tank mesocosms with comparable suspensions of white clay (17 - 20 mg/l) and no phytoplankton chlorophyll versus chlorophyll concentrations of 31 and 57 µg/l.

Additional experiments were conducted in tank mesocosms using different clays and phytoplankton conditions (Schalles et al., 2001). In one example, six stepwise additions of an Oklahoma red clay suspension were made to a tank containing a mixed chlorophyte phytoplankton bloom with 53 µg/l chl *a* (Figure 17). The final step resulted in a clay concentration of 55.4 mg/l. Similar to the white clay additions, reflectance again increased at all wavelengths. With red clay, however, the position of the green peak shifted 45 nm (from 546 to 591 nm), and the NIR peak shifted 4 nm (from 700 to 704 nm). We noted an observable color shift from green to reddish brown. In the red clay experiment, maximum reflectance reached 24.8% at 591 nm, which is less than the maximum values of 41.4% and 33.4% in the previous experiment in the low and high chlorophyll tanks with comparable white clay concentrations of approximately 57 mg/l (Figure 14).

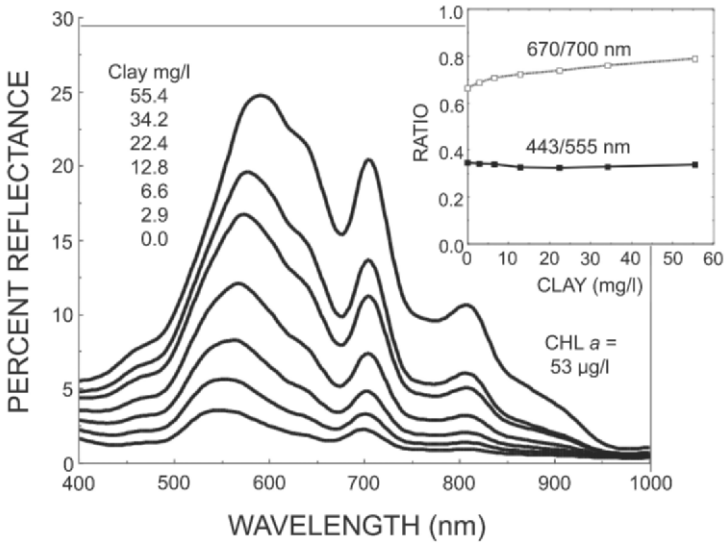

Figure 17. Reflectance spectra for a tank mesocosm experiment (Schalles et al., 2003) in which a red clay suspension was added stepwise to a tank containing a phytoplankton bloom of mixed Chlorophytes. Resulting clay concentrations are shown. Inset shows the effect of clay additions on band ratios for two chl *a* algorithms.

The red clay additions resulted in a much smaller change in the 443 to 555 nm ratio (-2.7%) and a moderate change (+ 19.2%) in the 670 to 700 nm ratio (see inset, Figure 17) when compared to white clay additions (Figure 15). The height of the NIR peak above a reference baseline from 675 to 750 nm increased from 0.9 to 6.2 percent reflectance (689% change). This NIR peak height calculation is an effective algorithm for chl *a* estimation in many Case 2 inland waters (Gitelson et al., 2000). In 17 separate mesocosm experiments with clay/algae interactions (Schalles et al., 2001), clay concentrations of 50 mg/l caused average changes of 9.4% in the 670 to 700 nm ratio and 325% in the NIR peak height above baseline. The clay additions caused a large shift to higher wavelengths in the green peak position. For clay additions of 50 mg/l, the average shift was +17.2 nm for the position of the green peak and +2.4 nm for the NIR peak.

7. CDOM Optics and Interference with Chlorophyll Algorithms

The term CDOM is an acronym for either colored (= coloured) or chromophoric dissolved organic matter. Both versions of the acronym refer to organic matter which strongly absorbs light in the ultraviolet and blue regions and less intensively at higher wavelengths. Chromophoric is a general term for molecular structures that absorb light. These light absorbing organic materials, largely composed of humic substances, are also variously named gilven (pale yellow color), gelbstoff, yellow substance, yellow organic acids, and humolimnic acid (Kirk, 1994). Their light absorbing properties are especially related to the presence of large molecular weight, aromatic humic and fulvic acids compounds. The chemical and light absorbing properties of CDOM are well investigated (Carder et al., 1989; Alberts and Filip, 1994; Schwarz et al., 2002). An

important, but sometimes overlooked, contribution of CDOM to spectral signatures is CDOM fluorescence. The CDOM emission wavelength is dependent on the excitation wavelength (Mobley, 1994), while CDOM fluorescence yield (a ratio of photons emitted to photons absorbed) is generally wavelength independent and varies from about 0.005 to 0.015.

CDOM substances largely originate from the decomposition of plant materials and are especially abundant in the discharges of streams and rivers with soft water, acidic chemistries and riparian zones with abundant plant biomass and productivity. Salt marsh and mangrove communities are also important sources of CDOM in the lower reaches of estuaries and other coastal habitats. CDOM concentrations are generally much lower in offshore waters and the open oceans (Carder et al., 1989) and originate from highly diluted inputs from land and from *in situ* phytoplankton production. CDOM dominates the water column optics in some estuaries and is responsible for the dark-stained, "blackwater" appearance of rivers such as the Rio Negro in Brazil and the Suwannee River in Florida. CDOM abundance is reported in either units of optical absorption of sample filtrate (ex. optical density or absorption units at a fixed wavelength in the ultraviolet or blue regions) or as carbon based, organic matter estimates (ex. dissolved organic carbon in mg/l), usually from oxidation of fixed carbon to carbon dioxide in carbon analyzer instruments.

At wavelengths greater than 300 nm, absorption by CDOM is inversely related to wavelength and is described by an exponential decay curve (Figure 18; see also Bricaud et al., 1981; Carder, 1989; Dekker, 1993; Schwarz et al., 2002). The magnitude of absorption at a single wavelength is highly correlated with CDOM concentration. However, the optical activity per unit carbon can vary in space and time and the slope of the semilogarithmic equation describing the absorption to wavelength relationship varies accordingly (Jerlov, 1976; Kirk, 1994). The average CDOM absorption from 28 estuarine and near shore stations on the Georgia coast was calculated in order to obtain a representative spectral curve (Figure 19). The average ABS_{440} value for these 28 stations was 2.12 m^{-1}. The average curve was then adjusted upward by one order of magnitude and downward by one and two orders of magnitude to create a family of curves. In turn, these curves were compared to the absorption spectrum of water (Figure 19). The curve for $ABS_{440} = 21.2$ exceeded water absorption values at all wavelengths below about 750 nm whereas the $ABS_{440} = 0.021$ curve exceeded water absorption only at wavelengths below 470 nm. Although the affect of CDOM absorption is strongest at lower wavelengths, this material can reduce reflectance signals at all visible wavelengths and into the lower NIR. When absorption of CDOM and water are combined (see inset, Figure 19), the water column can become highly absorptive across visible and NIR wavelengths. Note that the minimum combined absorption of CDOM and water shifts strongly to higher wavelengths with increasing CDOM concentrations (inset, Figure 19). At $ABS_{440} \sim 2$ m^{-1}, the minimum absorption is a rather broad region between 580 and 680 nm.

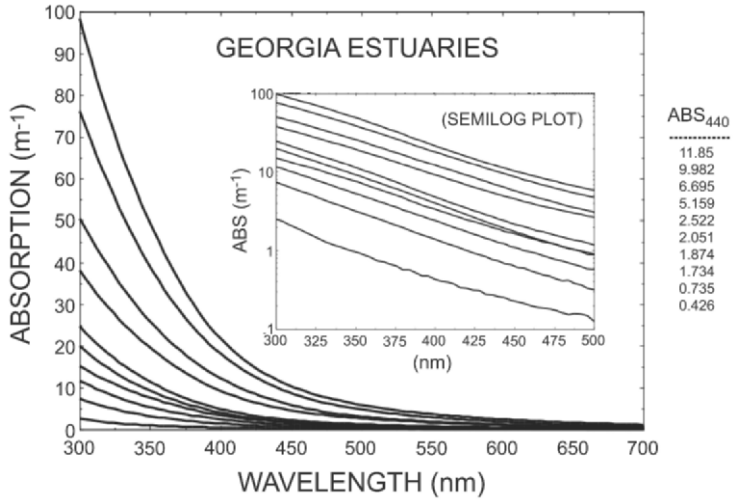

Figure18. Absorption spectra (300 - 700 nm) for dissolved organic matter (CDOM) in representative Georgia estuaries and offshore waters. Inset shows semilogarithmic plot of the same set of spectra. The respective ABS440 values (m^{-1}) for each of these spectra are shown to the right of the figure.

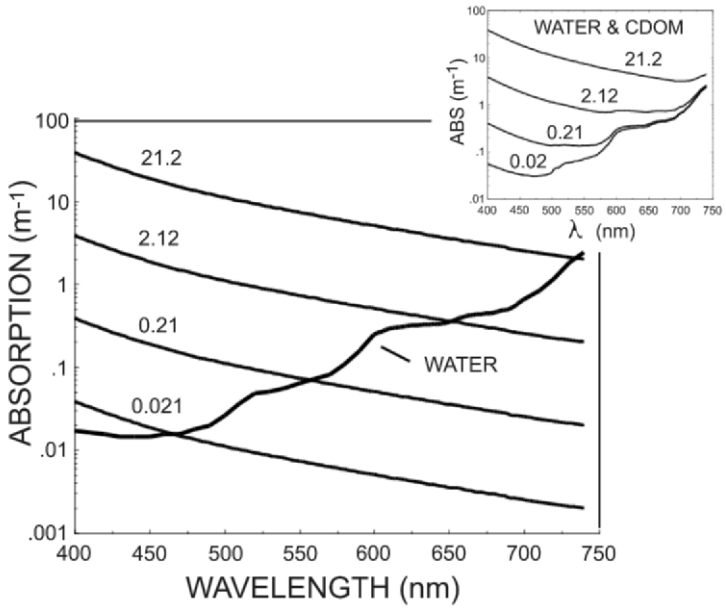

Figure 19. Modeled absorption spectra based on average absorption of Georgia sites (2.12 m^{-1} at 440 nm curve). The other 3 curves represent order of magnitude scaling. In turn, the family of CDOM absorption curves are compared to pure seawater. The inset shows the combined absorptions of CDOM and water for these four CDOM levels.

The combined water and CDOM absorption spectra shown in Figure 19 are compared in Figure 20 with selected total pigment absorption spectra from Figure 6. At chl *a* < 1 µg/l, pigment absorption activity is generally lower than the range of combined CDOM and water absorption typically encountered in coastal waters. At wavelengths below 550 nm and chl *a* > 1 µg/l, substantial overlap occurs between these different conditions. Only very high pigment levels in the red region result in higher absorption than the combined absorption of CDOM and water. When ABS_{440} (CDOM) exceeds 10 m^{-1}, the combined CDOM and water absorption exceeds the chl *a* = 100 µg/l absorption at all visible (PAR) wavelengths (Figure 20).

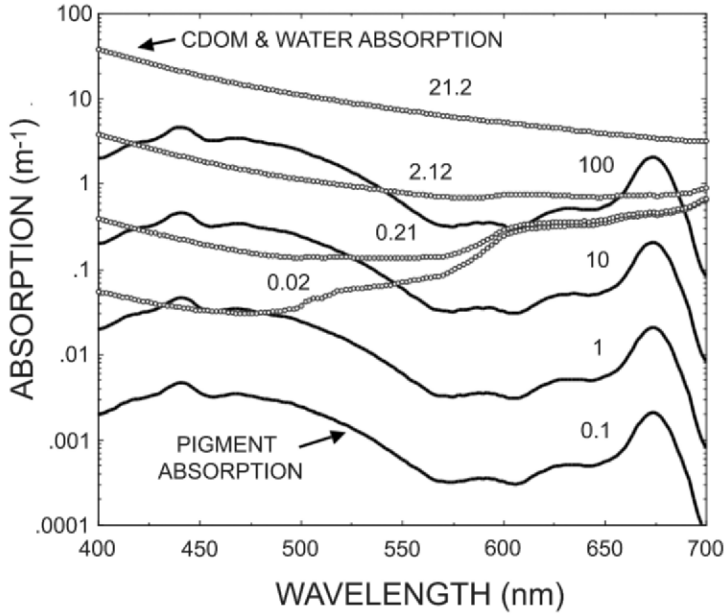

Figure 20. Combined water and CDOM absorption at four CDOM levels (see Figure 19) compared to algal pigment absorption at four levels (see Figure 6, pigment data from Bidigare et al., 1990). CDOM and chl *a* levels are shown for their respective spectral absorption curves.

The shapes and magnitude of combined water and CDOM absorption spectra have important implications for spectral features utilized in ocean color and other chlorophyll algorithms for Case 2 waters. An indoor experiment was conducted with a small (16.5 L) tank and involved stepwise additions of purified humic acid (as a sodium salt, Aldrich Chemical Corporation) to a lake water sample (Figure 21). Lake water was collected on September 12, 2004 from Carter Lake (Schalles et al., 1998b), immediately returned to the laboratory, and added to the measurement container. The lake water was dominated by the filamentous cyanobacterium *Anabaena*. Field Secchi transparency was 24 cm, and chl *a* was 116.3 µg/l. All tank reflectance measurements were completed within 2.5 hrs of sample collection. The ABS_{440} (CDOM) value for the lake water was 0.7 m^{-1}. Eighteen stepwise additions of humic acids brought the final CDOM absorption to 31.6 m^{-1}. Altogether, 1.328 g of humic acid (powder) was used, which achieved a final concentration of 80.24 mg/l. Tank water depth was 26 cm

(bottom not visible), and the tank was illuminated by a fiber optic illuminator (Cole-Parmer Series 41720) with a full VIS and NIR spectral emission. For each step of humic acid addition, aliquots of the tank water were removed and the powdered humic acid was thoroughly mixed with the aliquot. The aliquot, in turn, was thoroughly mixed into the tank before reflectance measures were taken. The lake water reflectance, prior to humic acid additions, was comparable to field measurements. The lake water prior to treatment had strong reflectance peaks centered at 566 and 708 nm and chlorophyll and phycocynanin induced reflectance minima (Figure 21). With each stepwise addition of humic acids, reflectance decreased within the VIS and lower NIR portions of the spectrum. There was no direct evidence that CDOM fluorescence caused an increased signal return at any wavelength, thus any CDOM fluorescence effect was masked by the increased absorption. Although all wavelengths were affected, reflectance decreases were most severe at the green and NIR peaks with the effects greatest, overall, at lower wavelengths (Figure 21). For example, the percent reflectance measures at 566 and 708 nm decreased by 4.79 and 4.63 respectively (or reductions in magnitude of 88.1% and 72.1%). In comparison, the percent reflectance measures at the 438 (Soret band) and 675 (Q band) minima decreased by 0.82 and 1.77 (or reductions of 59.3% and 61.7%). Declines in green peak heights were especially sensitive to the initial eight additions (up to $ABS_{440} \sim 8\ m^{-1}$). These data agree with an analytical model of water reflectance by Dekker (1993), in which he found that the minimum of phytoplankton reflectance at 676 nm was less affected by varying CDOM levels than was the NIR peak region at 706. Additionally, in the Netherlands shallow drainages that cut through peatlands exhibited high CDOM (ABS_{440} = 5.4 to 16.5 m^{-1}), and their reflectance spectra resembled those with the higher CDOM levels shown in Figure 21 (Rijkeboer et al., 1998). These workers also measured cases of extreme CDOM levels in fens (ABS_{440} up to 66 m^{-1}) , and found all reflectance in the visible range to be less than 1% with a strong shift of peak reflectance to NIR wavelengths.

Humic acid additions had a greater impact on the 443 to 555 nm algorithm ratio than on the 670 to 700 nm ratio (see inset, Figure 21). The 443 to 555 ratio was more sensitive at lower CDOM levels, corresponding to the large decreases in reflectance observed in green peak reflectance together with the less sensitive blue region, resulting in relatively large increases in the ratio. At ABS_{440} values of 4 and 8 m^{-1}, the 443 to 555 nm ratio increased by 63.6% and 110.2% over a starting value of 0.274. In comparison, the 670 to 700 nm ratio increased by only 0.9% and 1.9% at these intervals, from a starting value of 0.521. At the final ABS_{440} value of 31.6 m^{-1}, the 443 to 555 nm and 670 to 700 nm ratios increased by 223.6% and 26.0% respectively (inset, Figure 21). Based on these data, the chl *a* algorithms using green and blue wavelength ratios are far more sensitive to CDOM than the red and NIR algorithms. However, as shown above, this sensitivity would be dependent on the phytoplankton induced magnitude of the difference between green and blue band reflectance. Smaller differences between these bands should result in reduced sensitivity for chl *a* prediction.

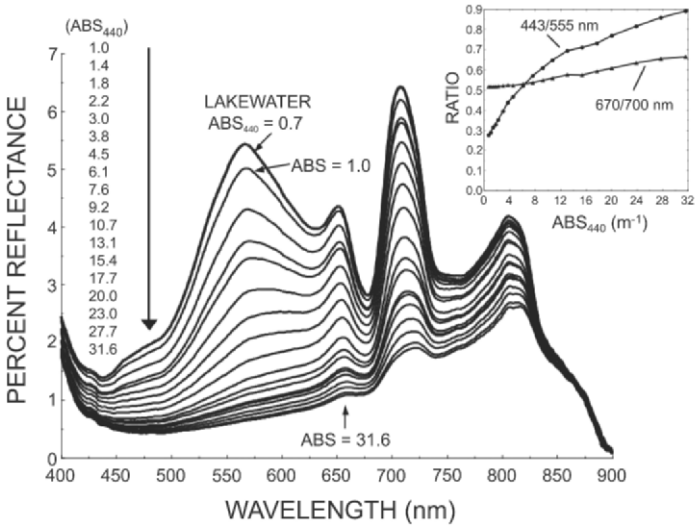

Figure 21. Effect of stepwise additions of humic acid on the spectral reflectance of a 16 liter lake water sample with an *Anabaena* sp. bloom held in a laboratory tank with lamp illumination (see text). Chl *a* concentration was 116.3 µg/l. Absorption (m^{-1}) values at 440 nm are shown for each step. Inset shows the effect of the humic acid additions on band ratios for two chl *a* algorithms.

Attenuation by CDOM is through absorption, although these materials intergrade with colloidal scale, detrital particles. The organic tripton (particulate detritus) fraction commonly has absorption spectra resembling the shape of CDOM absorption spectra (Dekker, 1993; Mobley, 1994; Rijkeboer, 1998; Brando and Dekker, 2003). The magnitude of organic tripton absorption may exceed that of CDOM in some coastal waters. In a transect of the St. Marys River in Georgia (Figure 22), CDOM dominated lower salinity, upstream stations (about 20-30 mg/l as dissolved organic matter) and organic tripton averaged about 2-3 mg/l in the same reach. However, organic tripton averaged about 10 - 15 mg/l in the lower estuary and CDOM levels were diluted to about 4-6 mg/l (Alberts et al., 2004). Typically, terrigenous organic matter is conservatively diluted in the estuarine mixing zone. At reduced flows and greatly increased residence times in the St. Marys estuary, CDOM dilution was non-conservative in the low to mid-salinity reach (Figure 22). Non-conservative mixing patterns were attributed to the formation of fine particulates as freshwater mixes with seawater (Alberts and Griffin, 1996). These particulates are commonly clay-detritus aggregates, with bacterial colonization and enriched nitrogen to carbon ratios (Lind and Davalos, 1990; Carlough, 1994). Many drainages have seasonal variations in discharge and CDOM concentrations. In Georgia coastal rivers, higher flow conditions are coincident with higher CDOM concentrations (Figure 22; also see Alberts and Filip, 1994), and the slope of the CDOM loading rate versus discharge relationship can exceed 1.0. Thus, higher discharge rates can create larger offshore plumes with higher CDOM concentrations. Estuarine and near shore waters may thus experience marked spatial and temporal variations in this optical constituent, resulting in strong effects on the water reflectance characteristics used to discriminate chlorophyll signals. Offshore waters generally have much lower CDOM levels than estuaries, with ABS_{440} values of

about 0.01 to 0.1 m^{-1} in open oceans, and about an order of magnitude greater in coastal waters (Kirk, 1994). At these levels, the effect of CDOM on chl *a* estimation should be greatly reduced.

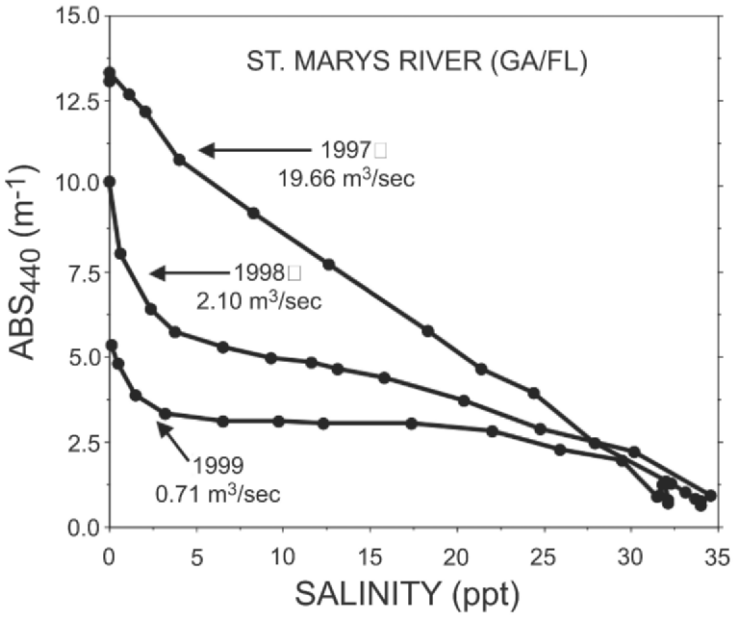

Figure 22. CDOM absorption values (m^{-1}) at 440 nm versus salinity for stations along the mixing zone and offshore plume of the St. Marys River on the Georgia/Florida border. Note the nearly conservative mixing during dilution in 1997, and non-conservative mixing in 1998 and 1999 at highly reduced flow conditions. Measurements of surface waters were taken each year in early summer (late June or early July). River flows (m^3/sec) are for a U.S. Geological Survey gauging station just above the estuarine mixing zone and the values represent averages of the daily values for the months of May and June in each year.

8. OACs and Reflectance Spectra Along Longitudinal Transects

Several examples from my research in Southeastern U.S. estuaries and near-shore waters illustrate the interactions of OACs and the composite impact of longitudinal gradients on water reflectance (Figures 23, 24). Sapelo Sound, at the north end of Blackbeard and Sapelo Islands, Georgia, receives only localized drainage. Sapelo Sound is relatively saline, has low levels of CDOM, and has less physical-chemical variation than the neighboring estuarine complex to the south, which is impacted by variability in flows of the Altamaha River. A transect from the Sound to adjacent near shore waters was made in July, 2000 aboard the R.V. Spartina (University of Georgia Marine Institute, Sapelo Island, Georgia). Salinity on the transect's six stations, beginning in mid-Sound, increased from about 30.9 to 35.3 ppt (Figure 23). Both chlorophyll and seston decreased by an order of magnitude (from 19.4 to 1.2 µg/l and 21.1 to 1.0 mg/l respectively). However, the percent of organic matter in the seston increased about 3 fold, from 26.7 to 74.2%. Secchi disk transparency increased from 0.78 to 5.30 m, while CDOM ABS_{440} values declined about two fold, from 0.43 to 0.20 m^{-1}

(not shown). As seen in Figure 23 water reflectance decreased with decreased scattering matter. The reflectance decrease was much stronger at the chl *a* red absorption band compared to the blue, Soret band. Peak reflectance was 4.8% at 580 nm in the Sound and declined to 2.1% at 548 nm offshore. The depth of the red absorption trough also declined sharply. Both the 443 to 555 nm and 670 to 700 nm ratios declined in a non-linear manner with increasing chlorophyll (see inset). The covariation of chl *a* and seston might suggest a Case 1 water condition. However, since the percentage of organic matter increased strongly along the transect, phytoplankton and detrital particles most likely dominated the offshore seston fractions while clays dominated the sound fraction (Figure 23).

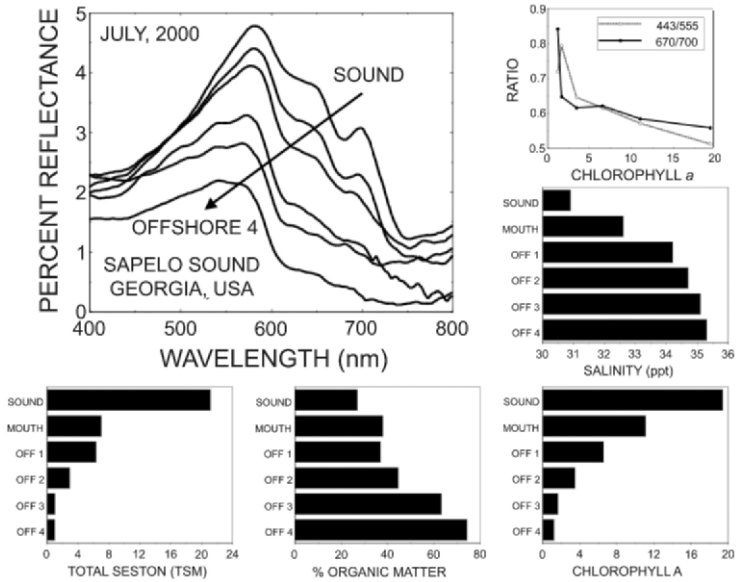

Figure 23. Reflectance curves, associated water measures, and calculated chl *a* band ratios at stations along a sampling transect from Sapelo Sound, Georgia to offshore waters of the Georgia Bight. Note: chl *a* values are µg/l, total seston values are mg/l dry weight.

A second longitudinal gradient example was measured in June, 2003 along a transect of 10 stations from the lower freshwater reach of the Edisto River to the mouth of St. Helena Sound in South Carolina (Hladik, 2004). In this transect, salinity increased from <0.1 to 27.2 ppt at the mouth of the Sound (Figure 24). Chlorophyll had a more complex pattern, with an initial decline from upriver values of 24.2 to 3.5 µg/l, a sharp increase to 26.5 in mid transect stations, and then a modest decline to about 18 µg/l in the Sound. Total seston generally increased and reached very high levels between mid transect and Sound stations. Seston averaged 5.7 mg/l in the first two upriver stations and 90.3 mg/l at the lower two Sound stations. CDOM (ABS_{440}) was very high upstream and decreased sharply along the mixing gradient, with the ABS_{440} values declining from 13.0 to 2.2 m^{-1}. Thus, the lowest CDOM absorption value in this transect was approximately five times the largest value for the previous Sapelo Sound transect. Reflectance generally increased along the_transect, related to increasing

scattering by seston and decreasing CDOM. Peak reflectance was 0.7% at about 700 nm at the upriver station and 4.4% at 648 nm at the mouth of the Sound. Depth of the Chl *a* red absorption trough was only partially correlated to chl *a* because the absorption of the high chl *a* concentration at the first, upriver station was largely masked by the high CDOM concentration (Figure 24) in a manner comparable to the masking effect at higher CDOM levels shown in Figure 21. Blue reflectance was low across the entire transect and very unresponsive to the large changes in both phytoplankton and total seston densities. Both ratio indices (443 to 555 nm and 670 to 700 nm) were relatively unresponsive and poorly linked to chl *a* concentrations (inset). In spite of nearly 5 times greater seston at the St. Helena Sound stations, peak reflectance values were roughly comparable with the Sapelo Sound stations, again illustrating the strong dampening effect of these elevated CDOM concentrations.

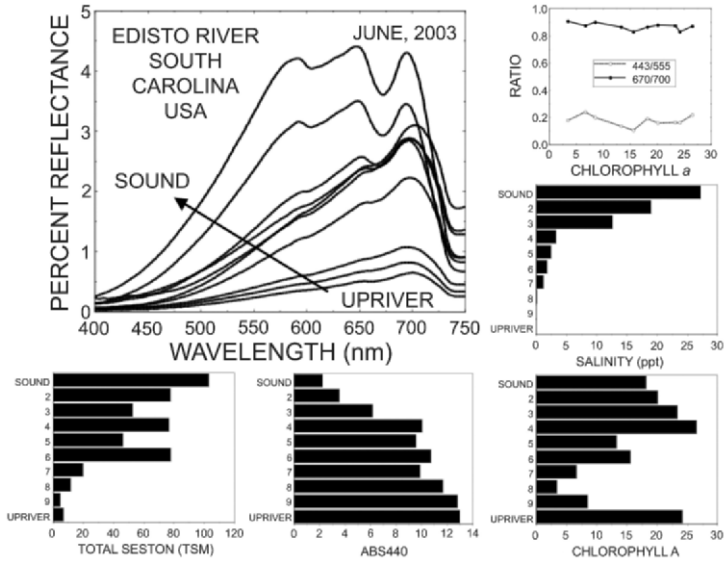

Figure 24. Reflectance spectra, associated water measures, and calculated chl *a* band ratios at stations along a sampling transect of the Edisto River in South Carolina. The transect extended from above the estuarine mixing zone to the mouth of St. Helena Sound, just south of Edisto Island. Note: chl *a* values are µg/l, CDOM absorption values at 440 nm are m^{-1}, and total seston values are mg/l dry weight.

9. The Reflectance Peak Near 700 nm: A Key Optical Feature in Case 2 Water Chlorophyll Algorithms

A confusing set of issues surrounds the interpretation of the reflectance maxima in the upper red and lower NIR spectral region (Figure 9). This feature is key to many of the emerging algorithms for Case 2 waters, and deserves additional consideration. Traditionally, ocean researchers equate this peak feature strictly to chlorophyll fluorescence (Carder and Steward, 1985; Gower and Borstad, 1990; Doeffer, 1993). Chlorophyll fluorescence is a well-studied phenomena that occurs universally in bacterial, protist, and higher plant chlorophylls (Butler, 1966; Rowan, 1989; Falkowski

and Raven, 1997). The principal emission band is sharply focused at 685 nm, although a broader and less intense band is also present and centered near 730 nm (Butler, 1966). Chlorophyll fluorescence is inelastic, and the 685 nm emission center is independent of the excitation wavelength (Mobley, 1994). However, the strength of chl *a* fluorescence is dependent on the wavelength of an absorbed photon. The 685 nm bandwidth, at 50% of full maximum, is about 25 nm (i.e. 672.5 to 696.5 nm).

Fluorescence yield (a ratio of photons detected within the emission spectra to photons absorbed within the excitation spectra) varies from < 0.01 to 0.10, and typically falls between 0.01 and 0.05 (Mobley, 1994). The yield is affected by the light regime, its spectral composition, and the physiological and nutritional state of photosynthetic cells as well as algal taxomony (Doerffer, 1993; Babin et al., 1996). Algal fluorescence is also subject to reabsorption by chlorophyll and some accessory pigments, as well as by surrounding water and absorbing CDOM and tripton materials (Pozdnyakov et al., 2002). Gower and Borstad (1990) calculated that percent reflectance for the red/NIR peak increases about 0.02% per µg/l chl *a*, although this relationship, and hence the fluorescence yield, decreased in areas of less thermal stratification and lower algal density. The fluorescence to chlorophyll relationship is quite non-linear, with higher sensitivity at lower chl *a*, allowing remote detection below 1 µg/l concentrations (Babin et al., 1996). In a long distance flightline across Case 1 waters in the North Atlantic, Yoder et al. (1992), demonstrated strong correlations between laser induced chlorophyll fluorescence and both the CZCS blue to green ratio index of reflected sunlight (r = 0.89) and the height above baseline (FLH, or fluorescence line height) algorithm (r = 0.96).

Gower et al. (1999) reexamined the nature of the red/NIR reflectance peak. They concluded that in instances of red tide blooms and coastal Case 2 water conditions, chlorophyll and water absorption, and particle scattering were all involved in the peak, along with fluorescence. One of the important features of the peak is a shift to higher wavelengths with increased chlorophyll concentration. Gitelson (1992) measured fluorescence spectra (range 640 to 750 nm) of water samples immediately after taking reflectance spectra. He found the position of the fluorescence peak remained constant at about 680 nm. However, the position of the *in situ* water reflectance peak varied from about 682 to 715 nm as chl *a* concentrations increased from 3 to > 100 µg/l. Vos et al. (1986) noted this same behavior, and concluded that the minimum in the combined absorption of chlorophyll and water accounted for the peak and its shift with increasing pigment concentration. This behavior is clearly seen in the graphical model of the combined absorptions of different chl *a* concentrations and water (Figure 6). The peak position of fluorescence emission is constant as chl *a* concentrations increases and it is difficult to reconcile a fluorescence explanation and the shift in reflectance peak position. Indeed, as the fluorescence emission builds with increasing chl *a* concentration, fluorescence should overtake water absorption in magnitude and maintain the reflectance peak position near 685 nm.

The large increases in the NIR peak height with increased white and red clay concentrations (Figures 14 and 17) demonstrate the important role of particle scattering in the presence of pigment and water absorption. However, the minimal effect (Figures 13 and 16) of increased concentrations of mineral tripton on the NIR reflectance peak position (Schalles et al., 2001) indicates that scattering is relatively unimportant in this peak position. The interpretation of the peak as a region of minimum, aggregate absorption along with coincident, wavelength independent scattering can thus be applied to both the mid-500 nm green peak and the NIR peak.

The issue of the relative importance of fluorescence to the NIR peak was explored in a set of observations where blocking filters were used to control the excitation and emission phenomena associated with fluorescence (Schalles et al., In Prep). The rationale were: 1) to block incident light in the spectral range known to stimulate chlorophyll fluorescence and observe whether a decrease in the NIR peak reflectance occurs; and 2) to block incident light in the red and near-infrared range of the peak and observe whether an underlying fluorescence pattern was apparent. In these observations, light from a quartz halogen projector lamp obliquely illuminated an 8 liter sample container. Measurements were made with a model SE590 spectroradiometer (Spectron Engineering) with a 6^{o} field of view foreoptic placed in nadir view 30 cm above the water surface. The instrument and foreoptics were calibrated for radiometric response using an integrating sphere at the NASA-Goddard SFC (Starks et al., 1995). The spectral composition of incident light was controlled with narrow pass filters placed over the projector lens. A "green" filter eliminated light below 620 nm and a red filter blocked light above 540 nm (Corion filters LS600-S-1288 and LL600-S-H942). The filters performed properly, but absorbed some light within their transmission ranges. Corrections for wavelength specific transmittance were applied to subsequent data measured with the filters. In the example presented here, an algal culture with a chl *a* concentration of 410 µg/l and a composition dominated by the green algae *Chlorella* and *Chlamydomas* sp. filled the sample container to a depth of 20 cm. When red and NIR light were excluded using the green narrow pass filter, a small emission feature, with a peak centered at the *in vivo* chlorophyll fluorescence wavelength of 685 nm, was evident (Figure 25). More importantly, the removal of red and NIR light by the green filter removed almost all of the NIR peak feature, indicating that most of the energy within the peak is reflectance and not fluorescence. When light energy below 600 nm, capable of exciting chlorophyll fluorescence, was excluded using the red filter, the NIR peak was strongly conserved, although the data indicated a small reduction of energy between about 670 and 720 nm (Figure 25). In other words, removal of most excitation energy for fluorescence had no significant effect on the shape or magnitude of the NIR peak.

In further analysis, the corrected radiance values obtained using the red narrow pass filter were subtracted from the unfiltered radiances, within the wavelength bounds of the NIR peak. The resultant curve had the same form as the fluorescence emission curve, but had almost twice the magnitude (see inset). Bandwidth (at 50% of full maximum) was 28 nm. Note that spectra isolated with both the red and green filters (inset) had maximum values at 685 nm, in agreement with the accepted wavelength for chlorophyll fluorescence, and that a shoulder (green filter spectra) or second, smaller peak (difference spectra) exists to the right of the NIR peak. The latter probably represents the secondary peak of chl *a* fluorescence near 730 nm (Butler, 1966). Although the precise magnitude of the contribution of chlorophyll fluorescence to the NIR peak remains uncertain in this case, it is clearly small in this example. Based on integration (data not shown) of the areas between 670 and 720 nm under the curves of the NIR peak (Figure 25 - unfiltered) and the chlorophyll emission feature (difference spectra - see upper curve of inset), fluorescence accounted for 7.9% of the energy of the entire NIR feature. However, at the NIR peak position, located at 709 nm, fluorescence accounted for only 3.7% of the total energy.

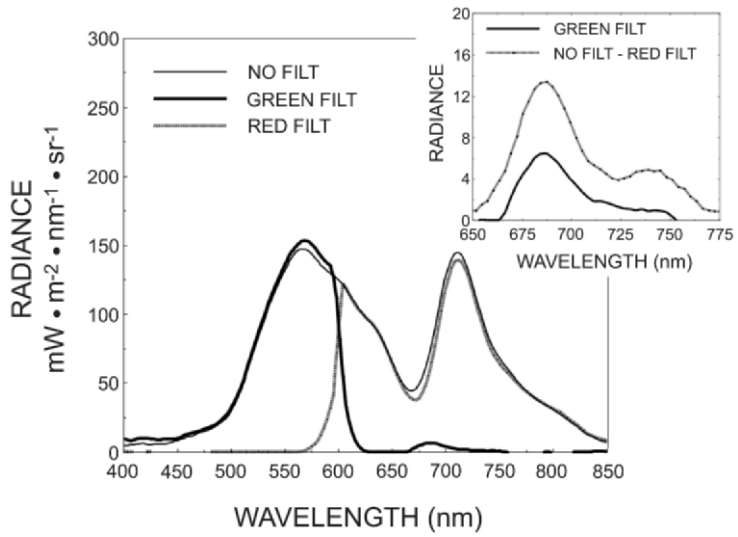

Figure 25. An experiment to isolate the contribution of algal chlorophyll fluorescence to the NIR reflectance peak of phytoplankton. The water leaving radiance, $L_w(O+)$, was measured at nadir above an algal culture in an 8 liter indoor tank with lamp illumination. Measurements were made with no filter place across the lamp source, with a narrow pass green (and blue) filter place across the lamp that prevented illumination of the tank at wavelengths above about 620 nm, and with a red filter that prevented lamp illumination below about 540 nm (indicated in figure). Data for the filter measurements was corrected for the transmission properties of each filter. The inset shows the curve of emissive, fluorescence energy measured with the green filter in place and for a second emission curve calculated from the difference between energy values without lamp filtration and with use of the red filter (see text for further information on the experiment).

Based on the evidence of field and laboratory measurements of reflectance and IOPs, the characteristics of pigment fluorescence, and modeling results which explicitly account for fluorescence yield, particle scattering, and water and pigment absorption, Gitelson (1992) concluded that algal scattering and absorption, coupled with the absorption properties of water, accounted for most of the NIR peak height and energy at chl *a* concentrations above 15 μg/l and that fluorescence is the dominant process below that threshold. The chlorophyll regime controls which processes are dominant. Thus, workers in oligotrophic Case 1 waters are correct in referring to the peak as a fluorescence phenomena but workers in eutrophic Case 2 waters are equally correct in referring to the peak as a scattering phenomenon governed by the interplay of chlorophyll and water absorption.

10. Comparison of Algorithms for Chlorophyll Estimation

As established above, the majority of passive (solar induced) remote sensing chlorophyll algorithms utilize: 1) a ratio of a band or bands within the chl *a* and carotenoid area of strong absorption between 440 and 510 nm versus the pigment minimum green region between at 550 to 555 nm; or 2) a ratio of a band in the NIR region of minimum combined water and pigment absorption and chlorophyll

fluorescence between 685 and 710 nm and the red chlorophyll absorption band between about 670 and 675 nm.

Examples of chlorophyll algorithms for two extreme conditions of Case 2 waters are shown in Figures 26 and 27 (inset). Carter Lake (Figure 7; Schalles et al., 1998b) is hypereutrophic and dominated by a diatom bloom in spring and during warm seasons by a filamentous cyanobacterial bloom. Thus, major shifts in pigment composition and quantity occur at this site throughout the year (Schalles and Yacobi, 2000). This shallow, groundwater fed lake is prone to wind re suspension of bottom sediments (largely detritus and clay) but has no turbid surface inflows. The best relationship between chl *a* and reflectance information was with the height of the NIR peak above a reference baseline extended between the red absorption trough at 675 nm and a region beyond pigment activity at 750 nm (Figure 26, inset). The relationship, based on measurements in a chl *a* range of 36 to 244 µg/l, was a first order, linear fit with an r^2 value of 0.83 (Table 1). This same relationship was the strongest predictor, as well, for a set of northern glacial lakes in Iowa, and for Lake Kinneret and Haifa Bay in Israel (Table 1; Gitelson et al., 2000). The regression coefficient for slope varied almost 50% between these diverse sites.

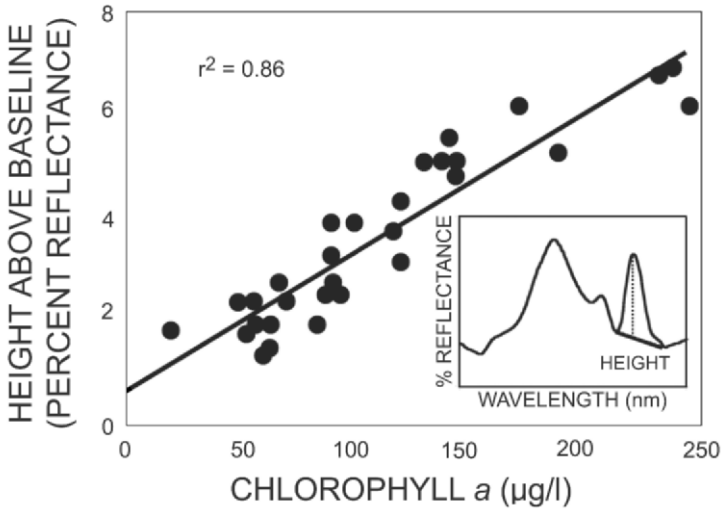

Figure 26. Chlorophyll *a* concentration versus NIR Height Above Baseline calculations from reflectance spectra in hypereutrophic Carter Lake, NE (Schalles et al., 1998). The inset graphically illustrates the basis for the height calculation.

Table 1. Comparison of retrieval algorithms for chlorophyll a in Case 1 and Case 2 waters. Rl is the reflectance value for a respective wavelength, and RLH is reflectance line height above baseline (see Figure 26), a_w=water absorption (m^{-1}), b_b = backscatter (m^{-1}), and int is the 10 nm bandwidth integral.

	Reference	r^2	Site(s)
Chl a = a + b*(RLH(670-750))	Schalles et al. (1998b)		
a = 1.77, b = 40.8		0.96	Lake Kinneret, Israel
a = 4.90, b = 47.2		0.93	Haifa Bay, Israel
a = 6.20, b = 31.8		0.83	Carter Lake, Nebraska, USA
Chl a = $10^{(0.4708-3.8469R+4.5338R2-2.4434R3)}$ - 0.0414 Where: R = (maximum value from R443, R490, or R510; see text) / R555	O'Reilly et al. (1998)	0.932	Global Oceans, some coastal waters
Chl a = 1.629 (R490/R55) $^{-2.551}$	D'Sa and Miller (2002)	0.81	Mississippi River plume - Gulf of Mexico
Chl a = log (-4.951*(R525/R554)) + 0.136	Vertucci and Likens (1989)	0.74	Adirondack Lakes, New York, USA

Table 1, cont'd.

	Reference	r^2	
Chl a = a + b*(R705/R662)	Kallio et al. (2003)		
a = -68.7, b = 108.5		0.98	Lake Lohjanjarvi, Finland
a = -77.1, b = 112.1		0.96	Lake Hiidenvesi, Finland
Chl a = -52.91 + 73.59*(R705/R678)	Thiemann and Kaufmann (2000)	0.89	Glacial Lakes, northern Germany
Chl a = 89* R705/R670 + 10*(R705/R670)^2 – 34	Mittenzwey et al. (1992)	0.98	Lakes and rivers, Germany
Chl a = R704/R672*(((a$_w$704+b$_b$)-a$_w$672)-b$_b^p$)/a*672 Where: a$_w$704=0.630; a$_w$672=0.415; a*672=0.0176 b$_b$776= 1.2*((R778*2.69)/ 0.187-R778); p =1.065	Gons (1999)	0.95	Lakes(Netherlands,China); Estuaries
Chl a = 56.7 + 161.0* -28.4*X^2 Where: X = ((intR660-670^{-1}) - (int R720-R730^{-1})) * (intR740-R750)	Dall 'Olmo et al. (2003)	0.94	Lakes and reservoirs, Nebraska, USA
Chl a = ((AVE R650+R700)-R675)/(AVE R440 + R550)	Hladik (2004)	0.80	Estuaries and near shore, Southeastern USA

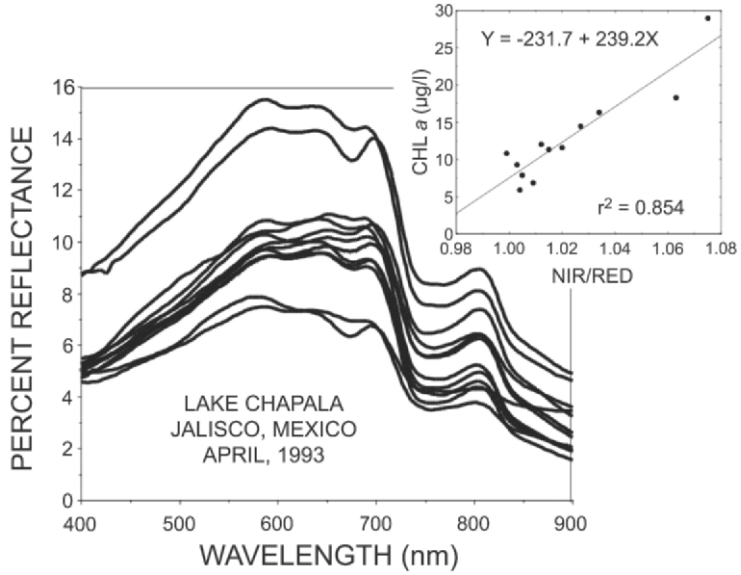

Figure 27. Reflectance spectra from twelve stations with high clay turbidities on Lake Chapala, Mexico in early April, 1993. The inset shows the relationship between measured chl *a* and a band ratio between the absolute height of the NIR peak and reflectance at the red, chlorophyll absorption trough near 675 nm.

The second example is Lake Chapala, a clay turbid tropical lake in the central highlands of Mexico (Lind et al., 1992). The largest natural lake in Mexico, Chapala has a surface area of about 1,100 km^2. The principal inflow is the Rio Lerma, which drains a watershed with a high degree of agricultural and industrial development. At low and at normal water levels, average depth varies from 4.5 to 7.2 m (Limón et al., 1989). Turbidity is primarily from fine clays (average 0.5 µ dia) and phytoplankton are typically light limited. In a detailed study carried out 1972 to 1984, Limón et al., 1989 reported an average Secchi depth transparency of 0.56 m and an average seston value of 29.7 mg/l (range 19-109). During one year of intensive study, chl *a* averaged 5.4 µg/l and the average annual primary production rate was only 80 g C/m^2 (Lind et al., 1992). In March and April, 1993, an optical study was conducted on this lake. Spectral reflectance was measured with the Spectron SE590 spectroradiometer at twelve stations, along with water sample collection for OAC estimates. The average and ranges for these stations were: chl *a* 12.8 µg/l (range = 5.9 - 29.0); seston = 84.0 mg/l (13.5 - 155.5); nephleometric turbidity = 47.7 NTU (33.4 - 67.0); and Secchi transparency = 0.24 m (0.09 - 0.52). The correlation between seston and chlorophyll was very weak (r = 0.105). Reflectance, measured at 50 cm above the surface, was high as a consequence of the high seston and turbidity (Figure 27). Maximum reflectance occurred near 585 nm, and ranged from 7.6 to 15.5%. The depth of the red chlorophyll absorption band varied in a general manner with chl *a* concentration. A second NIR peak, centered near 800 nm, represented a localized region of reduced water absorption in the presence of the high particle scattering. This second NIR peak is beyond the upper limits of algal pigment absorption activity. The best chl *a* regression model ($r^2 = 0.854$) was a ratio of

the value of the NIR peak (positioned near 695 nm) to red trough (Figure 27, see inset). No relationship existed between blue and green region band ratios and chlorophyll in the Lake Chapala stations.

Morel and Prieur (1977) proposed a reflectance ratio of 440 to 560 nm for discrimination of ocean chlorophyll, based on observed absorption maximum and minimum values found at these two wavelengths. This relationship was found to be inverse and nonlinear. Gordon and Morel (1983) attributed this nonlinear relationship to an increase in the ratio of phytoplankton (and, hence, chl *a*) to detrital byproducts with increasing chl *a* concentrations. They reasoned that higher chl *a* concentrations are typically found in nutrient stimulated conditions with vigorous algal population growth. Grazing pressures presumably reduce algal levels and increase both particulate and dissolved detrital products . Gordon and Morel (1983) also noted that absorption at 440 nm included a large accessory pigment component, and that variations in the chl *a* to accessory pigment ratio would add variation to the blue to green ratio algorithm and decrease the accuracy of chl *a* estimation. Aiken et al. (1995) found significant inter-province variation in the chlorophyll to carotenoid ratio but concluded that the two band, blue to green ratio approach was still robust and that regional calibrations were possible.

Chlorophyll algorithms have evolved over time. The Coastal Zone Color Scanner (CZCS), onboard the Nimbus 7 satellite, was launched in late 1978 and provided eight years of large scale, synoptic estimates of algal pigment. In 1981, the sensor performance became somewhat degraded (Evans and Gordon, 1994), but useful data were still generated. The instrument had bands for bio-optical monitoring at 443, 520, 550, and 670 nm, with 20 nm bandwidths. A two band ratio of 443 nm to 550 nm was calibrated and routinely used for chl *a* estimation, generating 66,000 CZCS chl *a* images. Two newer, operational sensors (SeaWiFS and MODIS) were also designed to use bands in the blue and green regions for ocean chlorophyll surveillance. These instruments have increased numbers of bands, improved calibration and atmospheric correction capabilities, and higher bit rates (for radiometric resolution). These new satellite programs have also greatly benefited from extensive, close range analyses of ocean pigments and water column optics since the era of CZCS. A recent multi-band, optimization procedure termed OC4 (for Ocean Color 4) utilizes 4 wavelengths for chl *a* estimation (O'Reilly et al., 1998; Table 1). The approach is termed the maximum band ratio (MBR) approach, based on comparing the ratios of 443 to 555 nm, 490 to 555 nm, and 510 to 555 nm. The largest value of these three ratios is used in a third order polynomial regression equation as the exponential term in a power function equation to best represent the sigmoidal relationship between chl *a* and band ratio calculations. In general, the 443 to 555 ratio is maximal below 0.3 μg/l, the 490 to 555 ratio is maximal between 0.3 and 1.5 μg/l, and the 510 to 555 ratio is maximal above 1.5 μg/l (O'Reilley et al., 1998). Their model was parameterized with data from the SeaWiFS Bio-Optical Algorithm Mini-Workshop (hereafter, SeaBAM). The data were collected from 919 ocean and coastal observation stations and had a chl *a* range of 0.019 to 32.79 μg/l. The multiband, ocean color algorithm approach continues to be refined for differing bio-optical ocean provinces and for attempts to utilize data from coastal waters tending toward Case 2 characteristics (Wernand et al., 1998; Stumpf et al., 2000; Sathyendranath et al., 2001; Yoo et al., 2002; D'Sa and Miller, 2003; Blondeau-Patissier et al., 2004). Carder et al. (1999) found a significant reduction in prediction errors when MODIS ocean color algorithms were adapted to three sets of oceanic bio-optical conditions.

Vertucci and Likens (1989) studied a group of 44 low to moderate productivity Adirondack mountain lakes in which the non-acid corrected chl *a* averages for five lake classes ranged from 0.3 - 4.8 μg/l. These lakes ranged from Case 1, low productivity, blue water lakes to Case 2 conditions with moderate chl *a*, variable CDOM, and colors ranging from gray-brown to yellow-green to brown. Optimization procedures were used to determine the best wavelength combinations within visible and lower NIR regions. In these lakes, a two band ratio of 525 nm to 554 nm (Table 1) performed significantly better than the band ratio of 443 to 550 nm. A bio-optical model using pigment, seston, and CDOM data produced model spectra very similar to their field spectra.

A majority of the semi-empirical algorithms for chlorophyll estimation in Case 2 waters utilize some variant of NIR peak height to chl *a* red absorption (Table 1). In a number of these studies, a simple two band ratio of the NIR peak, at either a fixed wavelength or at its maximum value is normalized to the minimum of reflectance at or near 675 nm. Kallio (2003) used a first order, linear equation with a band ratio of 705 to 662 nm to predict chlorophyll from AISA imagery data in two Finnish lakes with a chl *a* range of 6 to 70 μg/l. Thiemann and Kaufmann (2000) used a similar band ratio of 705 to 678 nm ratio to calibrate aerial hyperspectral imagery of lakes in northern Germany (chl *a* range of 5 to 350 μg/l). Mittenzwey et al. (1992) fit a second order polynomial to a band ratio of 705 to 670 nm in a set of lakes and rivers in Germany with a much wider chl *a* range of 5 - 350 μg/l (Table 1).

As discussed previously, Schalles et al. (1998b) and Gitelson et al. (2000) determined that a model using the height of the NIR peak above a normalizing baseline from 675 to 750 nm (Figure 26) was the best algorithm for eutrophic midwestern lakes in the United States and for Lake Kinneret and Haifa Bay in Israel. Gons (1999) modified the simple two band ratio (704 to 672 nm) approach using a bio-optical model. His approach required an inversion model for reflectance at 776 nm to estimate the backscatter coefficient b_b. The backscatter term became an adjustment for extra scattering by tripton particles, when combined with the respective water absorption coefficients for the 672 and 704 nm bands. This approach provided a robust chlorophyll prediction model for a diverse set of inland and coastal Case 2 waters with a chl *a* range of 2 to 994 μg/l. Gons et al. (2002) and Ruddick et al. (2004) modified this bio-optical model to utilize available bands on the MERIS satellite sensor. Dall 'Olmo et al. (2003) proposed a novel technique, with an algorithm derived from pigment estimation in terrestrial vegetation (Table 1). Their model was parameterized with Case 2 data from turbid and productive lakes and reservoirs in Nebraska, USA with a chl *a* range of 7 to 194 and a seston range of < 0.1 to 214 mg/l. Their model, as with Gons et al. (2002), uses a NIR band (740 to 750 nm) to compensate for backscatter by non-algal particles. However, their model uses a difference in the reciprocals of two bands (660 to 670 nm and 720 to 730 nm) to quantify pigment specific absorption activity and doesn't utilize the contrast in the NIR peak and chl *a* red trough features.

My laboratory recently participated in remote sensing studies at five National Estuarine Research Reserves. We examined water reflectance patterns within estuarine longitudinal mixing gradients and across watersheds and coastal provinces (Hladik, 2004; Schalles and Hladik, 2004). Optical measurements and analysis of OACs were made at Apalachicola Bay, Florida (October, 2002), Sapelo Island, Georgia and vicinity (January and August, 2003 and June, 2004), ACE Basin, South Carolina (June, 2003), Grand Bay, Mississippi (October, 2003), and Delaware Bay near Dover, Delaware (July, 2004). Reflectance was estimated from upwelling and downwelling signals collected simultaneously with a pair of fiber optic cables connected to separate

USB2000 spectroradiometers (Ocean Optics Corp., Dunedin, FL). Water samples were filtered for pigment and seston analysis and filtrate was used for CDOM absorption (Table 2). Algal pigments were extracted using 90% buffered acetone with a tissue grinder. Spectral data were collected and processed with the CDAP software package (CALMIT, University of Nebraska). We sampled 155 stations. Eleven stations, with ratios of total depth to Secchi transparency less than 1.5, were eliminated from analysis to avoid bottom reflectance biases. We measured a 600 fold range for chl *a*, a 200 fold range for ABS_{400}, and a 90 fold range for seston (Table 2). Correlations (r values) between OACs were quite low: seston and chl *a* = 0.274, seston and ABS_{440} = 0.031, and chl *a* and ABS_{440} = 0.045. In Figure 28, a conventional ocean color ratio (490 to 555 nm) was calculated for our data and compared to the SeaBAM data set used to parameterize the Ocean Color 4 algorithm (O'Reilly et al., 1998; see above). In the SeaBAM data set, the 490 to 550 nm ratio, fitted to a power function, yielded the highest r^2 value (0.915) of any band ratio pair and regression model in the SeaBAM data. The SeaBAM data had a strong negative correlation between the 490:555 ratio and chl *a*; however, our coastal data clearly did not (Figure 28). However, when a Case 2 algorithm was applied the r^2 value was much higher (discussed below). Some overlap occurred between individual values of the two data sets, particularly with the SeaBAM Chesapeake Bay stations (area A in the Figure) and a higher chlorophyll site in the Canadian arctic (area B; also see Figure 3 in O'Reilly et al., 1998). Cunningham et al. (2001) found similar divergence, using a reflectance band ratio of 443 to 555 nm, for Scottish fjord stations with high CDOM.

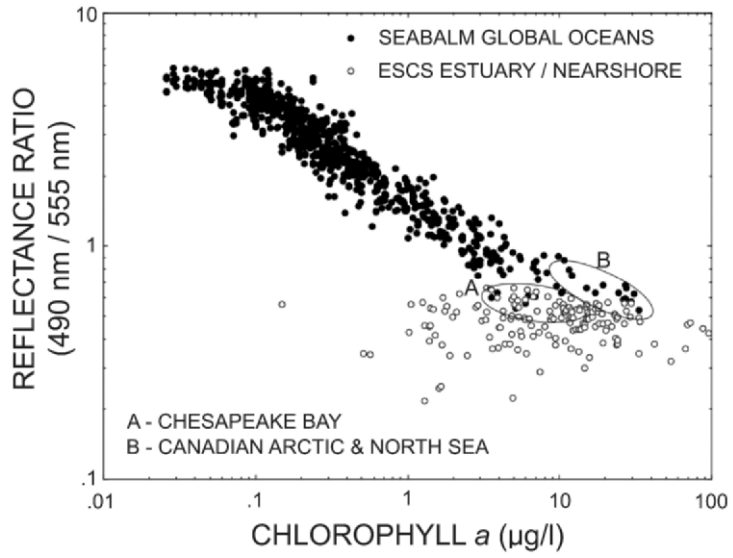

Figure 28. Chl *a* concentration versus water column reflectance ratio (490/553 nm) for the SEABAM data set (O'Reilly et al., 1998) used to calibrate the Ocean Color 4 (OC4) chlorophyll algorithm for the SEAWIFS satellite (closed circles) compared with ratio calculations from 144 sites in five National Estuarine Research Reserves in the eastern United States (open circles).

The series of Case 1 and 2 water algorithms listed in Table 1 were applied to our southeastern estuary data set. No relationships existed with any of the three Ocean

Color (OC4), two band ratios (Table 3; Figure 29a). There was also no relationship with the maximum band ratio values, where the numerator is the largest of the reflectance values at 443, 490, and 510 nm (Table 3). The simple 670 to 700 nm ratio had a relatively weak relationship to chl *a* (r^2 = 0.482; Table 3, Figure 29b). The bio-optical model of Gons et al. (2002) was revised for our data set, using reflectance and water absorption coefficient data at 674 nm and 698 nm, at the wavelengths best corresponding to our red trough and NIR values (Table 3). Although this model was robust in Northern Europe inland and coastal waters, we found a weaker relationship in our Atlantic Ocean and Gulf of Mexico coastal settings (r^2 = 0.322). The height of the NIR peak above a normalizing baseline between 675 and 750 nm was also unsatisfactory (r^2 = 0.355; Table 3).

Table 2. Summary of water analyses for 144 stations at four National Estuarine Research Reserves in the Southeastern United States (Hladik, 2004). Seston values are dry weight.

	Unit	Average	Median	Minimum	Maximum
chl *a*	µg/l	14.8	10.8	0.2	118.9
seston	mg/l	30.2	22.1	1.3	118.3
ABS_{440}	m^{-1}	4.9	3.7	0.1	21.1

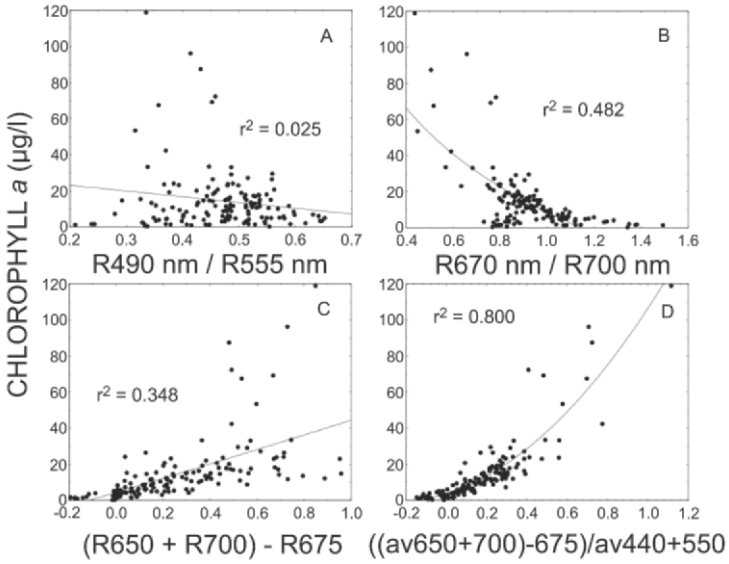

Figure 29. Comparison of four algorithms for chl *a* prediction. The data set is 144stations from five National Estuarine Research Reserves (Hladik, 2004; see Tables 1,2, and 3). (A) Ocean color ratio of 490 to 555 nm - see Figure 28, (B) Case 2 water ratio of 670to 700 nm, (C) new algorithm for depth of red trough below a normaling baseline from 650 to 700 nm, and (D) modification of this new algorithm using an average of reflectance at 440 and 550 nm as a denominator for correction of affects of tripton amplification and CDOM dampening.

The best fit between chl *a* and our data set for 144 stations was found for variants of a model which calculated the depth of the red trough feature, at 675 nm, below a

reference line between 650 nm and 700 nm, normalized as a ratio (average of reflectance values at 650 and 700 nm minus reflectance at 675 nm - see Table 3). The reference line position extends between the right edge of the shoulder near 650 nm and the vicinity of the NIR peak. The r^2 value for this algorithm was 0.348 (Table 3, Figure 29c). A second feature of the model was inclusion of reflectance data from lower wavelengths (440 and 550 nm) to normalize between the amplifying effects of tripton scattering and CDOM suppression of reflectance. The lower wavelength areas are more sensitive to these factors (Schalles et al., 1998a; Bowers et al., 2004), as described previously, although the factors also clearly influence the red and lower NIR wavelengths used in models for Case 2 waters. Second order, nonlinear equations best described the results of the model variants. When the reflectance at 550 nm was used as a denominator term, the regression r^2 improved from 0.775 (Table 3). A modest further improvement ($r^2 = 0.800$) was obtained when an average of reflectances at 440 and 550 nm was used in the denominator (Table 3, Fig. 29d). This later approach greatly reduced the correlation of residuals with elevated CDOM and seston conditions. The largest remaining residuals came from stations with higher chl *a* in several Georgia and Delaware estuaries (> 25 μg/l). We consider this model provisional and are collecting additional data in Chesapeake Bay, -Maryland in 2005 to increase the number of higher chlorophyll observations and to further test for robustness.

Table 3. A comparison of the relationships between various semi-empirical pigment algorithms and measured chl *a* (μg/l) in the ECSC study at four National Estuarine Research Reserves in the Southeastern United States (Hladik, 2004). See Table 1 for explanation of model terms.

MODEL	EQUATION	r^2
R443 / R555	Y = 14.6 - 0.0079X	0.000
R490 / R555	Y = 29.41 - 31.77X	0.025
R510 / R555	Y = 14.58 - 0.0073X	0.000
(max R443,R490,R510) / R555	Y = 15.04 - 0.701X	0.000
R670 / R700	Y = 8.56 - 145.72*LOG(X)	0.482
$(R698/R675*a_w698-b_b)-a_w674-b_b^{1.063}$	Y = -1.73 + 44.42X	0.322
NIR Peak Height (RLH R675 to R750)[1]	Y = 1.61 + 11.97X	0.355
(ave R650+R700) - R675	$Y = 4.34 + 38.84X + 1.139X^2$	0.348
(ave R650 + R700) - R675) / 555	$Y = 3.93 + 59.64X + 131.04X^2$	0.775
(aveR650+R700)-R675)/(aveR555+R550)	$Y = 3.72 + 34.92X + 67.63X^2$	0.800

[1] see Figure 26

11. Inverse Models to Relate Inherent Optical Properties and Chlorophyll Using Reflectance Spectra

The problems with site and temporal specificity in the above approaches using empirical and semi-analytical algorithms have motivated numerous researchers to develop analytical model approaches to link IOPs with measured AOPs, including reflectance spectra (Doerffer and Fischer, 1991; Dekker et al., 1997; Lahet et al., 2001; Sathyendranath et al., 2001; Pozdnyakov et al., 2002; Brando and Dekker, 2003; Bowers et al., 2004; Gege and Albert, this volume). If IOPs are well characterized and field reflectance data are carefully collected, inverse models can accurately retrieve water constituents (Bukata et al., 1995). However, the inverse approach is highly sensitive to errors in the measured radiometric variables, and even small errors may invalidate the inversions (Mobley, 1994).

An obvious problem is finding unique solutions for inversion problems in which optical water constituents and boundary conditions vary. Potentially, different sets of boundary and IOP conditions may lead to the same solution. Iterative, Monte Carlo techniques are typically used to find an optimal solution. Boundary conditions (atmospheric aerosols, water surface conditions, sun angle) may be very dynamic, particularly in coastal areas. High accuracy in atmospheric correction is crucial to success in discriminating water constituents, especially with satellite data (Brando and Dekker, 2003). The ability to differentiate optically shallow versus optically deep waters and the contribution of bottom reflectance is also important. Lee et al. (1999) developed a model which can derive bottom depths and water column properties from reflectance spectra. Heterogeneity in the IOPs is a further challenge. For example, differences in the slope of the absorption spectra of CDOM and detrital tripton (Bricaud et al., 1991; Carder et al., 1989; Dekker, 1993; Bowers et al., 2003), variability in pigment composition and cell packaging effects, and differences in volume scattering functions of the different classes of sestonic particles (Dekker et al., 1997) can all reduce the robustness of the assumed IOPs in coastal settings. Thus, it becomes necessary to measure and define specific IOPs (SIOPs) for a given site, and perhaps for a specific time (Brando and Dekker, 2003). Many of the inverse procedures reduce the optically active constituents to the three primary classes reviewed here (algal pigment, seston, and CDOM). However, these classes are often, themselves, complex mixes of constituents. Tidal fluxes, river plumes, and other physical mechanisms, which create spatial and temporal variability, can complicate the application of inversion models to large areas measured with satellite sensors (Doerffer et al., 1994). In many cases, it may not be practical for ship based researchers to synoptically measure water properties for IOP estimation. In fairness, this set of considerations often applies to the simpler, band ratio algorithms discussed above.

In spite of the serious constraints of applying inverse model approaches to coastal waters, a recent study of Moreton and Deception Bays in southeast Queensland, Australia demonstrated impressive results (Brando and Dekker, 2003). The authors used hyperspectral Hyperion Imaging Spectrometer data from the NASA Earth Observing One (EO-1) satellite. A MODTRAN-4 based atmospheric correction for coastal waters was developed. Validation of the atmospheric correction was confirmed by establishing good agreement between Hyperion hyperspectral reflectance and subsurface reflectance measured by a field instrument. The SIOPs of three classes of optical constituents (chl *a*, tripton, and CDOM) were measured and validated using

Hydrolight simulations. An efficient, direct solution of the inversion model was obtained using a matrix inversion method (MIM). The MIM was performed on each pixel of a Hyperion scene for Deception Bay. Maps of chl *a*, tripton, and CDOM were produced which had impressive accuracy and precision. Sensitivity analyses demonstrated that Hyperion could resolve constituents at the following intervals: chl *a* = 2.32 μg/l, tripton = 12.5 mg/l, and CDOM = 0.21 m^{-1}. The authors concluded that the procedure will require a much more thorough measurement of the spatial and temporal variation in SIOPs before accuracy can be further improved and the technique can be applied more broadly to optically diverse coastal waters.

12. Summary and Recommendations

Remote sensing procedures for chl *a* are becoming operational in coastal waters. However, these waters may quite possibly represent the most diverse optical conditions, in space and time, of any aquatic habitat. The ability to detect chl *a* in coastal waters is complicated by: 1) the large dynamic range of pigment in coastal waters; 2) a dominance of water optics by CDOM and/or tripton in many situations; 3) the spatial and temporal dynamics of coastal hydrology; 4) the diverse nature of the optical constituents and their SIOPs; 5) atmospheric aerosols and the requirement for accurate atmospheric corrections; 6) water density gradients and light and nutrient induced, non-uniform vertical distributions; 7) bottom reflectance and the diversity of benthic substrates; and 8) the problem of mixed pixels related to spatial resolution and contributions from shore zones. These challenges have required a redirection of optics research and remote sensing operational schemes for the Case 2 water conditions prevalent in most coastal settings.

The ability to detect chlorophyll in Case 2 waters requires, especially, hyperspectral data with the resolution to detect sometimes subtle pigment absorption bands, different accessory pigments, shoulders and peaks in reflectance spectra related to scattering and fluorescence activities, and good calibration and accuracy of instruments. The red and lower NIR spectral regions are often the most favorable for chl *a* detection in Case 2 waters because: 1) accessory pigments have minimal contribution to total absorption at these wavelengths; 2) CDOM and organic tripton have reduced absorption; and 3) the NIR peak feature in reflectance is more sensitive to the higher chl *a* ranges found in coastal waters. On the other hand, this wavelength range is less practical for lower chl *a* ranges because of dominance by water absorption.

Ocean color algorithms utilizing blue and green spectral bands are appropriate when Case 1 conditions occur in coastal waters. Pixel classification procedures may be required to make an initial examination of reflectance pattern and the selection of the most appropriate algorithm and parameterizations. However, the techniques for Case 2 water measurements reviewed in this chapter may also hold promise for the open oceans and other Case 1 waters such as large lakes (International Ocean-Color Coordinating Group, 2000). The challenges of Case 2 water optics have stimulated significant advancements in bio-optical modeling and insights into the interactions of optical constituents. Case 1 algorithms rely on an assumed covariance of constituents, whereas the techniques for relating Case 2 constituents to reflectance signals often require multivariate, non-linear models (International Ocean-Color Coordinating Group, 2000).

The best procedures to apply in a given situation often are decided by constraints of time, money, and resolution requirements of the user. In some cases, detection of

several general classes of water conditions and chl *a* levels may be sufficient. In other situations, change detection and the ability to resolve relatively small differences in chl *a* may be critical to bloom detection and reduction of damage to aquaculture operations, the ability to answer key ecological questions and improve modeling of primary production, and to meet regulatory criteria.

The problems remaining in order to achieve more routine, operational abilities to remotely measure chl *a* in coastal waters are relatively well identified. A number of research groups are actively engaged, as readily confirmed by the growing number of publications and technical presentations in Case 2 water optics research. Progress is evident, and further, rapid advancements are probable. Mobley (1994) was prescient in stating:

"The development of remote-sensing inversion algorithms for use in Case 2 waters scarcely has begun. As with other facets of the hydrologic optics of such waters, the remote sensing of case 2 waters will provide challenging research problems for a generation of scientists. "

13. Acknowledgements

I have greatly benefited from several collaborations in the past 15 years in both tank mesocosm experiments and field observations in inland and coastal waters. Donald Rundquist and Anatoly Gitelson at the University of Nebraska, Yosef Yacobi at the Kinneret Limnology Laboratory, Frank Schiebe at the USDA/ARS National Agricultural Water Quality Laboratory, and Jim Alberts and Monika Takacs at the University of Georgia Marine Institute at Sapelo Island were particularly generous with their time, intellectual engagement, and companionship. The Lake Chapala observations were conducted with Laura Davalos-Lind, Owen Lind, and Frank Schiebe. My work and perspectives have also been greatly enhanced from interactions with Pat Brezonik, Arnold Dekker, Giorgio Dall 'Olmo, Frank (Jerry) DeNoyelles, Sharon Dewey, Rolland Fraser, Luoheng Han, Giorgio Dall 'Olmo, Jeffrey Peake, Laurie Richardson, Robbi Stark, Patrick Starks, Richard Stumpf, and Bill Troeger. I've received support for the studies reported here from the NASA-Nebraska Space Grant Office, NOAA-NCCOS Environmental Cooperative Science Center, USEPA, visiting scientist appointments with the USDA/ARS National Agricultural Water Quality Laboratory, University of Georgia Marine Institute, and CALMIT-University of Nebraska-Lincoln. Scientists and technicians at the following NOAA National Estuarine Research Reserves provided outstanding support: ACE Basin, South Carolina, Apalachicola Bay, Florida, Delaware Bay, Delaware, and Grand Bay, Mississippi. I've worked closely with two Creighton University graduate students, Christine Hladik and Kim Whitman and benefited greatly from their enthusiasm, dedication, assistance, and questioning. The following individuals were particularly helpful in field and laboratory work and logistical support: Patrick A'Hearn, Ambrose Anoruo, Jennifer Arnhold, Wallace Bell, Jennifer Cherrier, Kevin Dillon, Chunlei Fan, Barbara Hayes, Chris Hiemstra, Rhonda Horner, Mark Huggins, Lisa Hughes, Charles Jagoe, David Kennedy, Amy Kroenke, Bryan Leavitt, Lee Edmiston, Mark Harwell, Stuart McNally, Christine Michaud, Katherine Milla, Albert Miller, Denise Lani Pascual, Heather Peterson, Kelli Peterson, Mary Price, Mike Reiter, Robert Scarborough, Jim Schalles, Amy Sheil, James Tycast, George Walker, Latrincy Whitehurst, Betty Winner, and Mark Woodrey. Finally, I'd like to thank my wife Nancy

Edwards Schalles for her generous support, encouragement, and patience. This paper is Contribution Number 949 from the University of Georgia Marine Institute.

14. References

Ackleson, S.G., and V. Klemas.1986. Two-flow simulation of the natural light field within a canopy of submerged aquatic vegetation. Applied Optics, 25:1129-1136.

Aiken, J., G.F. Moore, C.C. Trees, S.B. Hooker, and D.K. Clark. 1995. The SeaWiFS CZCS-Type Pigment Algorithm. SeaWiFS Technical Report Series , NASA Technical Memorandum 104566, Vol. 29. Goddard Space Flight Center, Greenbelt, Maryland.

Albert, A., and C.D. Mobley. 2003. An analytical model for subsurface irradiance and remote sensing reflectance in deep and shallow case-2 waters. Ocean Optics Express, 11: 2873-2890.

Alberts, J.J., and Z. Filip. 1994. Humic substances in rivers and estuaries of Georgia, USA. Trends in Chemical Geology, 1:143-162.

Alberts, J.J., and C. Griffin. 1996. Formation of particulate organic carbon (POC) from dissolved organic carbon (DOC) in salt marsh estuaries of the southeastern United States. Archives fur Hydrobiologie Special Issues, Advances in Limnology, 47:401-409.

Alberts, J.J., M. Takacs, and J.F. Schalles. 2004. Ultraviolet-visible and fluorescence spectral evidence of natural organic matter (NOM) changes along an estuarine salinity gradient. Estuaries, 27:297-311.

American Public Health Association. 1998. Standard Methods for the Examination of Water and Wastewater (20th edition). Section 1200 - Chlorophyll. American Public Health Association.

Andre, J.-M. 1992. Ocean color remote-sensing and the subsurface vertical structure of phytoplankton pigments. Deep Sea Research, 39:763-779.

Annenberg, P. 2000. Analysis of CASI data - a case study from the Archipelago of Stockholm, Sweden. Proceedings of the Sixth International Conference on Remote Sensing for Marine and Coastal Environments. University of Michigan Press., 2:149-156.

Antoine, D., J.-M. Andre, and A. Morel. 1996. Oceanic primary production 2. Estimation of global scale from satellite (coastal zone color scanner) chlorophyll. Global Biogeochemical Cycles, 10:57-69.

Babin, M., A. Morel, and B. Gentili. 1996. Remote sensing of sea surface Sun-induced chlorophyll fluorescence: consequences of natural variations in the optical characteristics of phytoplankton and the quantum yield of chlorophyll *a* fluorescence. International Journal of Remote Sensing, 17:2417-2448.

Barnard, A.H., W.S. Pegau, and J.R.V. Zaneveld. 1998. Global relationships of the inherent optic properties of the oceans. Journal of Geophysical Research, 103:24,955-24,968.

Bidigare, R.R., M.E. Ondrusek, J.H. Morrow, and D.A. Kiefer. 1990. *In vivo* absorption properties of algal pigments. SPIE Ocean Optics X: 1302:290-302.

Blondeau-Patissier, D., G.H. Tilstone, V. Martinez-Vicente, and G.F. Moore. 2004. Comparison of bio-physical marine products from SeaWiFS, MODIS, and a bio-optical model with *in situ* measurements from Northern European waters. Journal of Optics A: Pure and Applied Optics, 6:875-889.

Boss, E., and J.R.V. Zaneveld. 2003. The effect of bottom substrate on inherent optical properties: Evidence of biogeochemical processes. Limnology and Oceanography, 48:346-354.

Bowers, D.G., D. Evans, D.N. Thomas, K. Ellis, and P.J. le B. 2004. Williams. Interpreting the colour of an estuary. Estuarine, Coastal, and Shelf Science, 59:13-20.

Brando, V.E., and A.G. Dekker. 2003. Satellite hyperspectral remote sensing for estimating estuarine and coastal water quality. IEEE Transactions on Geosciences and Remote Sensing, 41:1378-1387.

Bricaud, A., A. Morel, and L. Prieur. 1981. Absorption by dissolved organic matter in the sea (yellow substances) in the UV and visible domains. Limnology and Oceanography, 26:43-53.

Brown, C.W., and J.A. Yoder. 1994. Coccolithophorid blooms in the global ocean. Journal of Geophysical Research, 99:7467-7482.

Bukata, R.P., J.H. Jerome, K.Y. Kondatyev, and D.V. Pozdnyakov. 1995. Optical Properties and Remote Sensing of Inland and Coastal Waters. CRC Press, Boca Raton, 362 pp.

Butler, W.L. 1966. Spectral characteristics of chlorophyll in green plants. In: (L.P. Vernon and G.R. Seely, editors) The Chlorophylls. Academic Press, pp. 343-380.

Carder, K.L., and R.G. Steward. 1985. A remote-sensing reflectance model of a red-tide dinoflagellate off west Florida. Limnology and Oceanography, 30:286-298.

Carder, K.L., R.G. Steward, G.R. Harvey, and P.B. Ortner. 1989. Marine humic and fulvic acids: Their effects on remote sensing of ocean chlorophyll. Limnology and Oceanography, 34:68-81.

Carder, K.L., F.R. Chen, Z.P. Lee, S.K. Hawes, and D. Kamykowski. 1999. Semianalytic Moderate-Resolution Imaging Spectrometer algorithms for chlorophyll *a* and absorption with bio-optical domains based on nitrate-depletion temperatures. Journal of Geophysical Research, 104:5403-5421.

Carlough, L.A. 1994. Origins, structure, and trophic significance of amorphous seston in a blackwater river. Freshwater Biology, 31:227-237.

Casazza, G, C. Silvestri, and E. Spada. 2003. Classification of coastal waters according to the new Italian water legislation and comparison to the European Water Directive. Journal of Coastal Classification, 9:65-72.

Cole, B.E., and J.E. Cloern. 1987. An empirical model for estimating phytoplankton productivity in estuaries. Marine Ecology Progress Series, 36:299-305.

Cracknell, A.P., S.K. Newcombe, A.F. Black, and N.E. Kirbu. 2001. The ABDMAP (Algal Bloom Detection, Monitoring and Prediction) Concerted Action. International Journal of Remote Sensing, 22:205-247.

Cunningham, A., P. Wood, and K. Jones. 2001. Reflectance properties of hydrographically and optically stratified fjords (Scottish sea lochs) during the Spring diatom bloom. International Journal of Remote Sensing, 22:2885-2897.

Curran, P.J., and E.M.M. Novo. 1988. The relationship between suspended sediment concentration and remotely sensed spectral radiance: A review. Journal of Coastal Research, 4:351-368.

D'Sa, E.J., and R.L. Miller. 2003. Bio-optical properties in waters influenced by the Mississippi River during low flow conditions. Remote Sensing of the Environment, 84:538-549.

Dall' Olmo, G., A.A. Gitelson, and D.C. Rundquist. 2003. Towards a unified approach for remote estimation of chlorophyll-a in both terrestrial vegetation and turbid productive waters. Geophysical Research Letters, 30:1938-1941.

Dekker, A.G. Detection of the Optical Water Quality Parameters for Eutrophic Waters by High Resolution Remote Sensing. 1993. Ph.D. Thesis. Free University, Amsterdam, The Netherlands, 212 pp.

Dekker, A.G., Z. Zamurovic-Nenad, H.J. Hoogenboom, and S.W.M. Peters. 1996. Remote sensing, ecological water quality modeling, and in situ measurements: a case study in shallow lakes. Hydrological Sciences, 41:531-547.

Dekker, A.G., H.J. Hoogenboom, L.M. Goddijn, and T.J.M. Malthus. 1997. The relation between inherent optical properties and reflectance spectra in turbid inland waters. Remote Sensing Reviews, 15:59-74

Doerffer, R. 1993. Estimation of primary production by observation of solar-stimulated fluorescence. ICES Marine Science Symposium, 197:104-113.

Doerffer, R., and J. Fischer. 1994. Concentrations of chlorophyll, suspended matter, and gelbstoff in case II waters derived from satellite coastal zone color scanner data with inverse modeling methods. Journal of Geophysical Research, 99:7457-7466.

Evans, R.H., and H.R. Gordon. 1994.Coastal zone color scanner "system calibration": a retrospective examination. Journal of Geophysical Research, 99:7293-7307.

Falkowski, P.G., and J.A. Raven. 1997. Aquatic Photosynthesis. Blackwell Science, 375 pp.

Gallegos, C.L., D.L. Correll, and J.W. Pierce. 1990. Modeling spectral diffuse attenuation, absorpion, and scattering coefficients in a turbid estuary. Limnology and Oceanography, 35:1486-1502.

Gallegos, C.L., and T.E. Jordan. 2002. Impact of the spring 2000 phytoplankton bloom in Chesapeake Bay on optical properties and light penetration in the Rhode River, Maryland. Estuaries, 25:508-518.

Gitelson, A. 1992. The peak near 700 nm on radiance spectra of algae and water: relationships of its magnitude and position with chlorophyll concentration. International Journal of Remote Sensing, 13:3367-3373.

Gitelson, A.A., J.F. Schalles, D.C. Rundquist, F.R. Schiebe, and Y.Z. Yacobi. 1999. Comparative reflectance properties of algal cultures with manipulated densities. Journal of Applied Phycology, 11:345-354.

Gitelson, A.A. Y.Z. Yacobi, J.F. Schalles, D.C. Rundquist, L. Han, R. Stark, and D. Etzion. 2000. Remote estimation of phytoplankton density in productive waters. Limnology and Lake Management - Archives fur Hydrobiolia, Special Issues, Advances in Limnology, 55:121-136.

Gons, H.J. 1999. Optical teledetection of chlorophyll a in turbid inland waters. Environmental Science and Technology, 33:1127-1132.

Gons, H.J., M. Rijkeboer, and K.G. Ruddick. 2002. A chlorophyll-retrieval algorithm for satellite imagery (Medium Resolution Imaging Spectrometer) of inland and coastal waters. Journal of Plankton Research, 24:947-951.

Gordon, H.R. 1997. Atmospheric correction of ocean color imagery in the Earth Observing System era. Journal of Geophyical Research, 102:17,081-17,106.

Gordon, H.R., and A.Y. Morel. 1983. Remote Assessment of Ocean Color for Interpretation of Satellite Visible Imagery. A Review. Springer-Verlag, New York. 114 pp.

Gower, J.F.R, and G.A. Borstad. 1990. Mapping of phytoplankton by solar-stimulated fluorescence using an imaging spectrometer. International Journal of Remote Sensing, 11:313-320.

Gower, J.F.R., R. Doerffer, and G.A. Borstad. 1999. Interpretation of the 685 nm peak in water-leaving radiance spectra in terms of fluorescence, absorption and scattering, and its observation by MERIS. International Journal of Remote Sensing, 20:1771-1786.

Hladik, C.M. 2004. Close range, hyperspectral remote sensing of Southeastern estuaries and an evaluation of phytoplankton chlorophyll *a* predictive algorithms. M.S. Thesis, Creighton University, Omaha, Nebraska, USA.126 pp.

Han, L., and D.C. Rundquist. 1994. The response of both surface reflectance and underwater light field to various levels of suspended sediments: Preliminary results. Photogrammetric Engineering and Remote Sensing, 60:1463-1471.

International Ocean-Color Coordinating Group. (S. Sathyendranath, Ed.) 2000. Remote Sensing of Ocean Color in Coastal, and Other Optically Complex, Waters. IOCCG Report Number 3, 140 pp.

Jahnke, R.A. 1996. The global ocean flux of particulate organic carbon: areal distribution and magnitude. Global Biogeochemical Cycles, 10:71-88.

Jassby, A.D., B.E. Cole, and J.E. Cloern. 1997. The design of sampling transects for characterizing water quality in estuaries. Estuarine, Coastal and Shelf Science, 45:285-302.

Jerlov, N.G. 1976. Marine Optics, 2nd edition. Elsevier Scientific Publishing Company.

Jordan, T.E., D.L. Cornell, J. Miklas, and D.E. Weller. 1991. Long-term trends in estuarine nutrients and chlorophyll, and short-term effects of variation in watershed discharge. Marine Ecology Progress Series, 75:121-132.

Jumars, P.A. 1993. Concepts in Biological Oceanography. Oxford University Press.

Kahru, M., and B.G. Mitchell. 1998. Spectral reflectance and absorption of a massive red tide off southern California. Journal of Geophysical Research, 103:21,601-21,609.

Kallio, K., S. Koponen, and J. Pulliainen. 2003. Feasibility of airborne imaging spectrometry for lake monitoring - a case study of spatial chlorophyll *a* distribution in two meso-eutrophic lakes. International Journal of Remote Sensing, 24:3771-3790.

Kirk, J.T.O. 1994. Light and Photosynthesis in Aquatic Ecosystems. 2nd Edition. Cambridge University Press.

Kitchen, J.C., and J.R.V. Zaneveld. 1992. A three-layered sphere model of the optical properties of phytoplankton. Limnology and Oceanography, 37:1680-1690.

Klemas, V., and D.F. Polis. 1977. Remote sensing of estuarine fronts and their effects on pollutants. Photogrammetric Engineering and Remote Sensing, 43:599-612.

Krijgsman, J. 1994. Optical remote sensing of water quality parameters - Interpretation of reflectance spectra. Ph.D. Thesis. Delft University of Technology, Delft University Press.

Lahet, F., S. Ouillon, and P. Forget. 2001. Colour classification of coastal waters of the Ebro river plume from spectral reflectances. International Journal of Remote Sensing, 22:1639-1664.

Lee, Z., K.L. Carder, C.D. Mobley, R.G. Steward, and J.S. Patch. 1998. Hyperspectral remote sensing for shallow waters. 1. A semianlaytical model. Applied Optics, 37:6329-6338.

Lee, Z., K.L. Carder, C.D. Mobley, R.G. Steward, and J.S. Patch. 1999. Hyperspectral remote sensing for shallow waters. 2. Deriving bottom depths and water properties by optimization. Applied Optics, 38:3831-3843.

Lefevre, N., A.H. Taylor, F.J. Gilbert, and R.J. Geider. 2003. Modeling carbon to nitrogen and carbon to chlorophyll *a* ratios in the ocean at low latitudes: Evaluation of the role of physiological plasticity. Limnology and Oceanography, 48:1796-1807.

Limón, J.G., O.T. Lind, D.S. Vodopich, R. Doyle, and B.G. Trotter. 1989. Long- and short-term variation in the physical and chemical limnology of a large, shallow, turbid tropical lake (Lake Chapala, Mexico). Archives fur Hydrobiologie, Supplement 83 (Monographische Beiträge), 57-81.

Lind, O.T., and L.O. Dávalos. 1990. Clay, dissolved organic matter, and bacterial interactions in two reservoirs. Archives fur Hydrobiologie, Ergebn. Limnologie, 34:119-125.

Lind, O.T., R. Doyle, D.S. Vodopich, B.G. Trotter, J. Gualberto Limón, and L. Dávalos-Lind. 1992. Clay turbidity: regulation of phytoplankton in a large, nutrient-rich lake. Limnology and Oceanography, 37:549-565.

Maritorena, S., A. Morel, and B. Gentili. 1994. Diffuse reflectance of oceanic shallow waters: influence of water depth and bottom albedo. Limnology and Oceanography, 39:1689-1703.

Mittenzwey, K.-H., S. Ullrich, A.A. Gitelson, and K.Y. Kondratiev. 1992. Determination of chlorophyll a of inland waters on the basis of spectral reflectance. Limnology and Oceanography, 37:147-149.

Mobley, C.D. 1994. Light and Water: Radiative Transfer in Natural Waters. Academic Press.

Morel, A. 1974. Optical properties of pure water and sea water. In: (N. Jerlov and E. Steemann Nielsen, editors) Optical Aspects of Oceanography. Academic Press, p. 1-24.

Morel, A., and L. Prieur. 1977. Analysis of variations in ocean color. Limnology and Oceanography, 22: 709-722.

Morrow, J.H., B.N. White, M. Chimiente, and S. Hubler. 2000. A bio-optical approach to reservoir monitoring in Los Angeles. Limnology and Lake Management - Archives fur Hydrobiolia Special Issues, Advances in Limnology, 55:171-191.

Muller-Karger, F.E., C.R. McClain, T.R. Fisher, W.E. Esaias, and R. Varela. 1989. Pigment distribution in the Caribbean Sea: observations from space. Progress in Oceanography, 23:23-64.

Munday, J.C., and P.L. Zubkoff. 1981. Remote sensing of blooms in a turbid estuary. Photogrammetric Engineering and Remote Sensing, 47:523-531.

Myers, MR, J.T. Hardy, C.H. Mazel, and P. Dustan. 1999. Optical spectra and pigmentation of Caribbean reef corals and macroalgae. Coral Reefs, 18:179-186

Odhe, T., and H. Siegel. 2001. Correction of bottom influence in ocean colour satellite images of shallow water areas of the Baltic Sea. International Journal of Remote Sensing, 22:297-313.

O'Reilly, J.E., S. Maritorena, B.G. Mitchell, D.A. Siegel, K.L. Carder, S.A. Garver, M. Kahru, and C. McClain. 1998. Ocean color chlorophyll algorithms for SeaWiFS. Journal of Geophysical Research, 103:24,937-24,953.

Paerl, H.W. 1988. Nuisance phytoplankton blooms in coastal, estuarine, and inland waters. Limnology and Oceanography, 33:823-847.

Pettersson, L.H., D. Durand, O.M. Johannessen, E. Svendsen, and H. Soiland. 2000. Satellite observations and model predictions of toxic algae blooms in coastal waters. Proceedings of the Sixth International Conference on Remote Sensing for Marine and Coastal Environments, 1:48-55.

Pozdnyakov, D., A. Lyaskovsky, H. Grassl, and L. Pettersson. 2002. Numerical modeling of transpectral processes in natural waters: implications for remote sensing. International Journal of Remote Sensing, 23:1581-1607.

Quinby-Hunt, M.S., A.J. Hunt, K. Lofftus, and D. Shapiro. 1989. Polarized-light scattering studies of marine *Chlorella*. Limnology and Oceanography, 34:1587-1600.

Richardson, L.L. 1996. Remote sensing of algal bloom dynamics. Bioscience, 46:492-501.

Rijkeboer, M., A.G. Dekker, and H. J. Gons. 1998. Subsurface irradiance reflectance spectra of inland waters differing in morphometry and hydrology. Aquatic Ecology, 31:313-323.

Ritchie, J.C., F.R. Schiebe, C.M. Cooper, and J.A. Harrington, Jr. 1994. Chlorophyll measurements in the presence of suspended sediment using broad band spectral sensors aboard satellites. Journal of Freshwater Ecology, 9:197-206.

Rowan, K.S. 1989. Photosynthetic Pigments of Algae. Cambridge University Press.

Ruddick, K., Y. Park, and B. Nechad. 2003. MERIS imagery of Belgian coastal waters: mapping of suspended particulate matter and chlorophyll-*a*. Proceedings of MERIS user workshop, Frascati, Italy, ESA SP-249.

Rundquist, D.C., J.F. Schalles, and J.S. Peake. 1995. The response of volume reflectance to manipulated algal concentrations above bright and dark bottoms at various depths in an experimental pool. Geocarto International, 10:5-14.

Sathyendranath, S., L. Lazzara, and L. Prieur. 1987. Variations in the spectral values of specific absorption of phytoplankton. Limnology and Oceanography, 32:403-415.

Sathyendranath, S., G. Cota, V. Stuart, H. Maass, and T. Platt. 2001. Remote sensing of phytoplankton pigments: a comparison of empirical and theoretical approaches. International Journal of Remote Sensing, 22:249-273.

Schalles, J.F., F.R. Schiebe, P.J. Starks, and W.W. Troeger. 1997. Estimation of algal and suspended sediment loads (singly and combined) using hyperspectral sensors and experiments. Proceedings of the Fourth International Conf. on Remote Sensing of Marine and Coastal Environments, 1:247-258.

Schalles. J.F., A.T. Sheil, J.F. Tycast, J.J. Alberts, and Y.Z. Yacobi. 1998a. Detection of chlorophyll, seston, and dissolved organic matter in the estuarine mixing zone of Georgia coastal plain rivers. Proceedings of the Fifth International Conference on Remote Sensing for Marine and Coastal Environments, 2:315-324.

Schalles, J.F., A.A. Gitelson, Y.Z. Yacobi, and A.E. Kroenke. 1998b. Estimation of chlorophyll a from time series measurements of high spectral resolution reflectance in an eutrophic lake. Journal of Phycology, 34:383-390b.

Schalles, J.F. and Y.Z. Yacobi. 2000. Remote detection and seasonal patterns of phycocyanin, carotenoid, and chlorophyll pigments in eutrophic waters. Limnology and Lake Management - Archives fur Hydrobiolia Special Issues, Advances in Limnology, 55:153-168.

Schalles, J.F., D.C. Rundquist, and F.R. Schiebe. 2001. The influence of suspended clays on phytoplankton reflectance signatures and the remote estimation of chlorophyll. Vehr. Intern. Verein. Limnol. 27: 3619-3625.

Schalles, J.F., F.R. Schiebe, C.M. Hladik, F.R. Schiebe, J.F. DeNoyelles, and D.R. Rundquist. An analysis of the red/NIR fluorescence and reflectance peak (690-720 nm) of phytoplankton blooms. (in prep.)

Schiebe, F.R., J.A. Harrington, Jr., and J.C. Ritchie. 1992. Remote sensing of suspended sediments: the Lake Chicot, Arkansas project. International Journal of Remote Sensing, 13:1487-1509.

Schwarz, J.N., P. Kowalczuk, S. Kaczmarek, G.F. Cota, B.G. Mitchell, M. Kahru, F.P. Chavez, A. Cunningham, D. McKee, P. Gege, M. Kishino, D.A. Phinney, and R. Raine. 2002. Two models for absorption by coloured dissolved organic matter (CDOM). Oceaonologia, 44:209-241.

Siegel, D.A., M. Wang, S. Maritorena, and W. Robinson. 2000. Atmospheric correction of satellite ocean color imagery: the black pixel assumption. Applied Optics, 39:3582-3591.

Smith, R.C., and K. Baker. 1981. Optical properties of the clearest natural waters. Applied Optics, 20: 177-184.

Starks, P.J., F.R. Schiebe, and J.F. Schalles. 1995. Characterization of the accuracy and precision of spectral measurements by a portable, silicon diode array spectrometer. Photogrammetry and Remote Sensing, 61:1239-1246.

Stumpf, R.P, R.A. Arnone, R.W. Gould, P. Martinolich, V. Ransibrahmanakul, P.A. Tester, R.G. Steward, A. Subramaniam, M. Culver, and J.R. Pennock. 2000. SeaWiFS ocean color data for U.S. Southeast coastal waters. Proceedings of the Sixth International Conference on Remote Sensing for Marine and Coastal Environments, 1:25-27.

Talling, J.F. 1993. Comparative seasonal changes, and inter-annual variability and stability, in a 26-year record of total phytoplankton biomass in four English Lake District basins. Hydrobiologia, 268:65-98.

Thiemann, S., and H. Kaufmann. 2000. Lake water quality monitoring using hyperspectral airborne data – a multitemporal approach. Proceedings of the Sixth International Conference on Remote Sensing for Marine and Coastal Environments, 2:157-164.

Walsh, J.J. 1991. Importance of the continental margins in the marine biogeochemical cycling of carbon and nitrogen. Nature, 350:53-55.

Wang, M., D.R. Lyzenga, and V.V. Klemas. 1996. Measurement of the optical properties in the Delaware Estuary. Journal of Coastal Research, 12:211-228.

Wernard, M.R., S.J. Shimwell, S. Boxall, and H.M. van Aken. 1998. Evaluation of specific semi-empirical coastal colour algorithms using historic data sets. Aquatic Ecology, 32:73-91.

Vertucci, F.A., and G.E. Likens. 1989. Spectral reflectance and water quality of Adirondack mountain region lakes. Limnology and Oceanography, 34:1656-1672.

Vos, W.L., M. Donze, and H. Buiteveld. 1986. On the reflectance spectrum of algae in water: the nature of the peak and 700 nm and its shift with varying concentration. Communications on Sanitary Engineering and Water Management, Number 7, TU Delft, The Netherlands, 29 pp.

Yoder, J.A., J. Aiken, R.N. Swift, F.E. Hoge, and P.M. Stegmann. 1992. Spatial variability in near-surface chlorophyll a fluorescence measured by the Airborne Oceanographic LIDAR (AOL). Deep Sea Research II, 40:37-53.

Yoo, S.-J., H.-C. Kim, J.-a. Lee, and M.-O. Park. 2002. Validation of chlorophyll algorithm in Ulleung Basin, East/Japan Sea. Korean Journal of Remote Sensing, 18:35-42.

Zaneveld, J.R.V., D.M. Roach, and H. Pak. 1974. The determination of the refractive distribution of oceanic particulates. Journal of Geophysical Research, 79:4091-4095.